


# Semiparametric bivariate extreme-value copulas<sup>\*</sup>

Javier Fernández Serrano<sup>1</sup>

 <https://orcid.org/0000-0001-5270-9941>

## Abstract

Extreme-value copulas arise as the limiting dependence structure of component-wise maxima. Defined in terms of a functional parameter, they are one of the most widespread copula families due to their flexibility and ability to capture asymmetry. Despite this, meeting the complex analytical properties of this parameter in an unconstrained setting remains a challenge, restricting most uses to models with very few parameters or nonparametric models. In this paper, we focus on the bivariate case and propose a novel approach for estimating this functional parameter in a semiparametric manner. Our procedure relies on a series of transformations, including Williamson's transform and starting from a zero-integral spline. Spline coordinates are fit through maximum likelihood estimation, leveraging gradient optimization, without imposing further constraints. Our method produces efficient and wholly compliant solutions. We successfully conducted several experiments on both simulated and real-world data. Specifically, we test our method on scarce data gathered by the gravitational wave detection LIGO and Virgo collaborations.

**Keywords:** extreme-value copula, bivariate copula, semiparametric model, Pickands dependence function, Williamson's transform, compositional spline

2020 MSC: 62H05, 62H12, 62-08

## 1. Introduction

Copulas allow modelling multivariate dependencies independently from the distribution of the corresponding margins. Sklar's theorem [1] states that any bivariate cumulative distribution function (CDF)  $H$  can be decomposed as  $H(x, y) = C(F(x), G(y))$ , where  $F$  and  $G$  are the first and second margin CDFs from  $H$  and  $C$  is the so-called copula function. The latter is defined over  $[0, 1]^2$  and has the analytical properties of a restricted bivariate joint CDF with uniform margins on  $[0, 1]$ . The uniqueness of  $C$  is ensured provided that  $F$  and  $G$  are continuous; otherwise, it is uniquely determined on  $\text{Ran}(F) \times \text{Ran}(G)$ . Conversely, given univariate CDFs  $F$  and  $G$  and a copula  $C$ ,  $H$  is a joint CDF with margins  $F$  and  $G$ .

We can retrieve the unique part of a copula from a CDF  $H$  utilizing the *quasi-inverses* [1]  $F^{[-1]}$  and  $G^{[-1]}$  of  $F$  and  $G$ , respectively:  $C(u, v) = H(F^{[-1]}(u), G^{[-1]}(v))$ . This procedure generates *implicit* copulas from known bivariate CDFs, for instance, the Gaussian copula or the Student's copula [2]. Other copulas have *explicit* forms, most notably Archimedean [3], extreme-value [4] or archimax copulas [5]. One or more functional parameters characterize these *meta-families*. Particular instantiations of such functions give rise to parametric families like Clayton's or Frank's (Archimedean), Tawn's (extreme-value) or Gumbel's (both Archimedean and extreme-value).

<sup>\*</sup>This research did not receive any specific grant from funding agencies in the public, commercial, or not-for-profit sectors. Declarations of interest: none.

Email address: javierfdez\_90@hotmail.com (Javier Fernández Serrano)

<sup>1</sup>Independent researcher.

*Extreme-value copulas.* Consider a sequence  $\{(X_{1,i}, X_{2,i})\}_{i=1}^{\infty}$  of independent and identically distributed random 2-vectors with copula  $C$  and continuous margins. Let us build the sequence of partial maxima  $\{(M_{1,n}, M_{2,n})\}_{n=1}^{\infty}$ , where  $M_{j,n} = \max_{i \leq n} \{X_{j,i}\}$ . The copula of the  $n$ -th element is given by  $(u, v) \mapsto C(u^{1/n}, v^{1/n})^n$ . Then, a copula  $C$  is said to be an extreme-value copula (EVC) if it is the weak limit of the previous sequence, i.e.,  $\lim_{n \rightarrow \infty} C^*(u^{1/n}, v^{1/n})^n = C(u, v)$ , for all  $(u, v) \in [0, 1]^2$  and some underlying copula  $C^*$ . It turns out that  $C$  is an EVC iff it can be expressed as

$$C(u, v) = \exp \left\{ \log(uv) A \left[ \frac{\log(u)}{\log(uv)} \right] \right\}, \text{ for } u, v \in (0, 1)^2, \quad (1)$$

where  $A : [0, 1] \rightarrow \mathbb{R}$ , known as the Pickands function (PF), satisfies the following two constraints:

1.  $\max\{t, 1 - t\} \leq A(t) \leq 1$ , for all  $t \in [0, 1]$ .
2.  $A$  is convex.

The first constraint confines the graph of  $A$  to a triangular subset of  $[0, 1]^2$  and makes  $\text{Ran}(A) \subset [1/2, 1]$ . It can also be replaced with an equivalent constraint [6] concerning the behaviour of  $A$  at the endpoints, namely  $A(0) = A(1) = 1$ ,  $A'(0^+) \geq -1$  and  $A'(1^-) \leq 1$ . The lines  $\{(t, 1 - t) : t \in [0, 1]\}$  and  $\{(t, t) : t \in [0, 1]\}$  are called the *support* lines of the PF. The lower bound  $\max\{t, 1 - t\}$  yields  $C(u, v) = \min\{u, v\}$ , the comonotonic copula, whereas the upper bound,  $A \equiv 1$ , corresponds to the independence copula  $C(u, v) = uv$ . Figure 1 depicts all these elements. On the other hand, the convexity constraint can be replaced by  $A''(t) \geq 0$  for all  $t \in [0, 1]$  whenever  $A$  is twice differentiable [6].

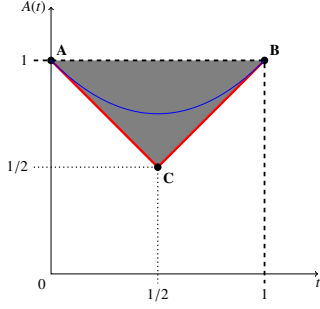


Figure 1: PF geometry. The admissible region for its graph appears in grey. Support lines show in red. Points **A**, **B** and **C** will be referenced later on when describing our method. An example of PF, namely  $A(t) = t^2 - t + 1$ , is drawn in blue.

It is easy to check that any convex combination of PFs results in a PF. Also, given a PF  $A$ , the change of variable  $\bar{A}(t) = A(1-t)$  yields a PF too. In fact, it can be shown that the symmetry of  $C$  in (1), meaning  $C(u, v) = C(v, u)$ , is equivalent to the symmetry of  $A$  with respect to the  $\{t = 1/2\}$  axis [7], i.e.,  $A(t) = \bar{A}(t)$  for all  $t \in [0, 1]$ . For this reason, some authors [7] define EVCs equivalently by taking  $\log(v)/\log(uv)$  as the argument of  $A$  in (1). Taking both properties into consideration, it follows that  $\hat{A}(t) = (A(t) + \bar{A}(t))/2$  is symmetrical and, hence, the subsequent copula will be exchangeable.

For EVCs, correlation coefficients like Kendall's tau and Spearman's rho can be computed as integrals involving  $A$  [8]. Even simpler, Blomqvist's beta [9] and the upper tail index can be expressed in terms of  $A(1/2)$  as, respectively,  $\beta = 4^{1-A(1/2)} - 1$  and  $\lambda = 2(1 - A(1/2))$ . We see both measures are related through  $\beta = 2^\lambda - 1$  and that  $\beta = \lambda = 1$  is attained iff  $A(1/2) = 1/2$ , which is equivalent to  $A$  producing the perfect positive dependence (comonotonic) copula. Except for the case of comonotonicity, EVCs do not exhibit lower tail dependence.

**Example 1.** The function  $A(t) = t^2 - t + 1$  in Figure 1 is a PF since  $A(0) = A(1) = 1$ ,  $A'(0) = -1$ ,  $A'(1) = 1$  and  $A''(t) = 2$  for all  $t \in (0, 1)$ . Additionally,  $A(t) = A(1-t)$ , thus the subsequent EVC is exchangeable. It can also be checked that it is the lowest degree polynomial PF such that  $A(1/2) = 3/4$ , thus producing  $\beta = \lambda = 1/2$ .

The PF can yet be expressed [6] as

$$A(t) = \int_0^1 \max\{t(1-z), z(1-t)\} d\mathcal{H}(z),$$

where  $\mathcal{H}$  is the so-called *spectral* measure on  $[0, 1]$ : a finite measure satisfying  $\int_0^1 z d\mathcal{H}(z) = 1$ . Furthermore, under absolute continuity of  $A'$  [6],  $\mathcal{H}$  admits a decomposition

$$\mathcal{H}(B) = \mathcal{H}_0 \mathbf{1}_B(0) + \int_B \eta(z) dz + \mathcal{H}_1 \mathbf{1}_B(1), \quad (2)$$

where  $\mathbf{1}_B$  denotes the indicator function on  $B$ ,  $\eta = A''$  almost everywhere on  $(0, 1)$ ,  $\mathcal{H}_0 = 1 + A'(0^+)$  and  $\mathcal{H}_1 = 1 - A'(1^-)$ .

Neither the original constraints of  $A$  nor the spectral measure ones of  $\mathcal{H}$  can be easily attained through conventional approximation methods like polynomials or splines. Instead, the

Family	$A_\theta(t)$	$\theta$ range
Gumbel	$[t^\theta + (1-t)^\theta]^{1/\theta}$	$[1, \infty)$
Galambos	$1 - [t^{-\theta} + (1-t)^{-\theta}]^{-1/\theta}$	$(0, \infty)$
Hüssler-Reiss	$\varphi(t) + \varphi(1-t)$ , $\varphi(t) \equiv t \Phi\left(\theta + \frac{1}{2\theta} \log\left(\frac{t}{1-t}\right)\right)$	$(0, \infty)$

Table 1: Main one-parameter EVC families [8]. The  $\Phi$  in the Hüssler-Reiss designates the standard normal CDF. The above families are all symmetrical. Khoudraji's procedure provides an alternative for introducing asymmetry.

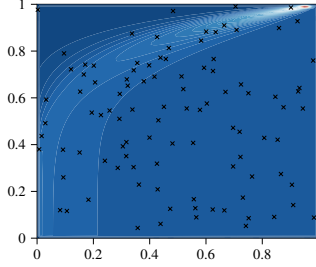


Figure 2: Sample-density plot of an instance of the Tawn family (Gumbel family with asymmetry induced by Khoudraji's procedure) with parameters  $\theta = 5.0$ ,  $\alpha = 0.5$  and  $\beta = 0.1$ .

most well-known EVCs belong to one-parameter symmetrical families. Table 1 includes some examples.

The following procedure by Khoudraji [10] and described in [7] allows obtaining asymmetrical copulas from symmetrical ones. Given a copula  $C$  (not necessarily symmetrical [11]) and  $\alpha, \beta \in (0, 1)$ , we can build a new copula  $C_{\alpha, \beta}(u, v) = u^{1-\alpha} v^{1-\beta} C(u^\alpha, v^\beta)$ . Moreover, if  $C$  is an EVC, the corresponding  $C_{\alpha, \beta}$  will also be an EVC, with PF given by

$$A_{\alpha, \beta}(t) = (1-t)(1-\alpha) + t(1-\beta) + w A\left(\frac{t\beta}{w}\right), \quad (3)$$

where  $w = (1-t)\alpha + t\beta$ . In general, if  $C$  is symmetrical,  $C_{\alpha, \beta}$  will be asymmetrical whenever  $\alpha \neq \beta$ . The asymmetrical extensions by means of (3) of the Gumbel and Galambos families in Table 1 are known as the Tawn and Joe copula families, respectively [7]. Figure 2 shows an example of the former.

*Organization.* This paper proposes a novel approach for constructing a PF that can flexibly fit data. Our method produces highly parameterized approximations that meet all the constraints for a PF. It does so, relying on a few weak assumptions and remaining computationally tractable.

In section 2, we will provide a review of previous EVC modelling approaches. Next, section 3 is entirely devoted to our method, addressing both theoretical and practical issues. We will later test our method on a simulation study (SS) and real-world data in section 4. Finally, in section 5, we provide further comments on the performance and general possibilities of our method and, eventually, propose some future lines of work in section 6.

## 2. Related work

Vettori, Huser, and Genton provide a comprehensive literature review on EVCs, comparing different methods and fo-

cusing on relevant aspects, such as constraint compliance and applicability to higher dimensions [12]. The most relevant methods fall into one of two categories, namely nonparametric or parametric estimation. In general, nonparametric models demonstrate greater flexibility than parametric ones, especially when dealing with asymmetrical data, at the expense of higher variance. In dimensions higher than two and with mild asymmetry, parametric models, using Khoudraji's asymmetric extension, perform well against nonparametric ones.

One of the first estimators for the PF was proposed by Pickands himself [13] in the context of bivariate survival analysis [14]. However, [13] is almost surely non-convex over  $[0, 1]$  [14]. Several authors have proposed corrections for [13] to be convex. Pickands himself proposed in [13] to use the greatest convex minorant of the original estimator, which remains one of the most practical and efficient approaches of its kind.

Perhaps the most widespread nonparametric method is due to Capéraà, Fougères, and Genest [15], from which it borrows its name CFG. They observe that given a random sample  $\{(U_i, V_i)\}_{i=1}^n$  from an EVC with PF  $A$ , the transformation  $Z_i = \log U_i / \log(U_i V_i)$  is distributed according to

$$H(z) = z + z(1-z) \frac{A'(z)}{A(z)}. \quad (4)$$

One can empirically estimate  $H$  with some  $\tilde{H}$  and solve (4) for an estimator

$$\tilde{A}(t) = \exp \left\{ \int_0^t \frac{\tilde{H}(z) - z}{z(1-z)} dz \right\}. \quad (5)$$

The estimator  $\tilde{A}$  is not convex in general. Jiménez, Villadharce, and Flores propose two modified versions of the CFG that do satisfy the convexity constraint [14].

According to [12], most estimation methods until the early 2010s are variants of either Pickands', CFG or both. More recent advances have focused on polynomials and splines. For instance, Guillotte and Perron study the conditions under which a polynomial, expressed in Bernstein form, is a PF [6]. Marcon et al. use Bernstein-Bézier polynomials to enforce some PF constraints [16]. Cormier, Genest, and Nešlehová use constrained quadratic smoothing B-splines to develop a compliant PF in a nonparametric fashion using the R `cobs` package [17]. Previously, Einmahl and Segers had introduced a compliant nonparametric estimator of the spectral measure that required constrained optimization [18].

The work by Vettori, Huser, and Genton shows that despite EVCs having been around for a long time, some of the most relevant and accepted methods fail to meet all the constraints required by the PF even for the bivariate case. Semiparametric approaches, like the one introduced by Hernández-Lobato and Suárez for Archimedean copulas [19], have not been explored in the context of EVCs.

We believe that the research community is currently focusing on multivariate extensions [20] and paying less attention to the bivariate case, which is broadly considered a solved problem. However, we consider that a more fundamental construc-

tion is still missing in this context; one for which a large number of parameters can be fit in a fully unconstrained manner without breaking the PF assumptions. The work by Kamnitsi et al. [8] suggests that the bivariate EVC family is not as narrow as could be initially thought, especially if asymmetry comes into play. For that matter, we believe that splines are a powerful tool. Notwithstanding, contrary to other authors, we aim to use them not as a convenient shape-preserving estimator but as the core of a semiparametric model like [19].

Bacigál explores the use of Williamson's transform in the context of copulas [21]. As we will show in Section 3, modelling a PF is similar to modelling an Archimedean generator from a certain point of view. McNeil and Nešlehová use Williamson's transform in their study of  $d$ -monotone Archimedean generators [3, 22]. Charpentier et al. also use it to pursue a more general family of multivariate Archimax copulas [5]. The work by Fontanari, Cirillo, and Oosterlee, on the use of Lorenz curves as non-strict Archimedean generators [23], suggests that the research community is on the verge of coming at a similar use of Williamson's transform in the context of EVCs.

### 3. Proposal

In the following sections, we will cover (i) the construction of a new semiparametric EVC, some (ii) convergence and (iii) association results, (iv) its estimation and (v) simulation and, finally, (vi) a possible solution to one of its limitations.

#### 3.1. Construction

Our method addresses both constraints of the PF by geometrically transforming the problem into one for which we know a straightforward solution.

##### 3.1.1. Affine transformation

The support lines of the PF resemble a pair of coordinate axes if conveniently rotated and scaled. Let  $M$  be the unique 2-dimensional affine transformation mapping  $(0, 1)$ ,  $(0, 0)$  and  $(1, 0)$  to  $(0, 1)$ ,  $(1/2, 1/2)$  and  $(1, 1)$ , respectively.  $M$  and  $M^{-1}$  take the form

$$M(x, w) = \frac{1}{2} \begin{pmatrix} 1 + x - w \\ 1 + x + w \end{pmatrix}, \quad M^{-1}(t, a) = \begin{pmatrix} t + a - 1 \\ a - t \end{pmatrix}. \quad (6) \quad (7)$$

Under certain conditions, the inverse mapping  $M^{-1}$  transforms the graph of a PF,  $\{(t, A(t)) \mid t \in [0, 1]\}$ , into the graph of a 2-monotone function  $W$  defined on  $[0, 1]$  and satisfying  $W(0) = 1$  and  $W(1) = 0$ . Here, 2-monotone stands for non-increasing and convex [3, 5]. Such a  $W$  is more tractable than the original PF. Figures 1 and 3 show the transition from one to the other.

Note that for a twice differentiable function  $W$  with the above boundary constraints, 2-monotonicity is equivalent to  $W'(x) \leq 0$  and  $W''(x) \geq 0$ , for all  $x \in (0, 1)$ . This smoothness assumption simplifies the demonstration of the following proposition.

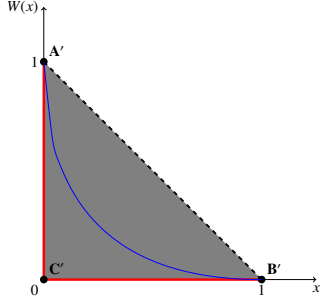


Figure 3: The geometry of a 2-monotone function derived from a PF. The graph of the function  $W$  ranges from  $A'$  to  $B'$  and never crosses the dashed line segment between these two points. The rotated version of the PF in Figure 1,  $W(x) = x - 2\sqrt{x} + 1$ , is drawn in blue.

**Proposition 1.** *Let all the upcoming functions be twice differentiable on  $(0, 1)$ . By means of (6) and its inverse (7), there is a one-to-one correspondence between PFs  $A$  satisfying  $A(t) > 1 - t$ , for all  $t \in (0, 1/2]$ , and 2-monotone functions  $W$  defined on  $[0, 1]$  and satisfying  $W(0) = 1$ ,  $W(1) = 0$ . Namely,  $A$  can be obtained from  $W$  as*

$$\begin{cases} t(x) = \frac{1}{2}(1 + x - W(x)) \\ A(t(x)) = \frac{1}{2}(1 + x + W(x)) \end{cases} \quad (8)$$

and conversely,  $W$  from  $A$ , as

$$\begin{cases} x(t) = t + A(t) - 1 \\ W(x(t)) = A(t) - t \end{cases}, \quad (9)$$

where both  $t(x)$  and  $x(t)$  are automorphisms of  $[0, 1]$ .

*Proof.* Let  $W$  be as defined above. We will see that  $A$  as defined in (8) is a PF with the additional constraint above.

First, note that  $t(0) = 0$ ,  $t(1) = 1$ . By continuity of  $W$ , this implies that  $\text{Ran}(t) = [0, 1]$ . Then, for  $t(x)$  to be an automorphism of  $[0, 1]$ , it suffices to see that it is one-to-one. Let us suppose that  $t(x_1) = t(x_2)$  for some  $x_1, x_2 \in [0, 1]$ ,  $x_1 < x_2$ . Then,  $W(x_2) - W(x_1) = x_2 - x_1 > 0$ , which leads to a contradiction with  $W$  being non-increasing. Therefore,  $t(x)$  is an automorphism of  $[0, 1]$ , so  $A$  in (8) is well-defined as a function of a single variable  $t \in [0, 1]$ .

Next, letting the support lines  $t_+(x) \equiv t(x)$  and  $t_-(x) \equiv 1 - t(x)$ , it is easy to check that  $t_{\pm}(x) = \frac{1}{2}(1 \pm x \mp W(x))$  and, since both  $x$  and  $W(x)$  are non-negative (otherwise  $W$  would not be non-increasing, with  $\text{Ran}(W) = [0, 1]$ ), we may conclude  $A(t(x)) \geq \max\{t_+(x), t_-(x)\}$ . Furthermore,  $A(t(x)) > 1 - t(x)$  for all  $x \in (0, 1] \supset (0, 1/2]$ .

Finally, some easy calculations show that

$$A'(t(x)) = \frac{1 + W'(x)}{1 - W'(x)}, \quad (10) \quad A''(t(x)) = \frac{4 W''(x)}{(1 - W'(x))^3}. \quad (11)$$

Since  $W'(x) \leq 0$  and  $W''(x) \geq 0$ , it follows that  $A''(t) \geq 0$ , for all  $t \in (0, 1)$ , and hence  $A$  is convex. This finishes the proof that (8) defines a PF such that  $A(t) > 1 - t$ , for all  $t \in (0, 1/2]$ .

Conversely, let  $A$  be a PF with the latter additional constraint. We will similarly show that  $W$  as defined in (9) is 2-monotone and satisfies  $W(0) = 1$  and  $W(1) = 0$ .

First, note that  $x(0) = 0$  and  $x(1) = 0$ . By continuity of  $A$ , this implies that  $\text{Ran}(x) = [0, 1]$ . Then, for  $x(t)$  to be an automorphism, it suffices to see that  $x(t)$  is one-to-one. Let us suppose that  $x(t_1) = x(t_2)$  for some  $t_1, t_2 \in [0, 1]$ ,  $t_1 < t_2$ . This implies that  $[A(t_2) - A(t_1)]/(t_2 - t_1) = -1$  and, since  $A$  is convex, we must conclude that  $A(t) = 1 - t$  for all  $t \in (t_1, t_2]$ . Clearly,  $t_2 \leq 1/2$ , because  $1 - t < t$  if  $t > 1/2$  and, on the other hand,  $A(t) \geq \max\{t, 1 - t\}$ . Therefore,  $(t_1, t_2] \subset (0, 1/2]$ , which leads to a contradiction with  $A(t) > 1 - t$  over  $(0, 1/2]$ . Hence,  $x(t)$  must be one-to-one and, all in all, an automorphism of  $[0, 1]$ . This, in turn, means that  $W$  in (9) is well-defined as a function of a single variable in  $[0, 1]$ .

Next, it is easy to check both  $W(0) = 1$  and  $W(1) = 0$ , bearing in mind that  $A(0) = A(1) = 1$ .

Finally, differentiating in (9), we get, for  $t \in (0, 1)$ ,

$$W'(x(t)) = \frac{A'(t) - 1}{A'(t) + 1}, \quad (12) \quad W''(x(t)) = \frac{2 A''(t)}{(1 + A'(t))^3}. \quad (13)$$

Since  $A(t) > 1 - t$  for  $t \in (0, 1/2]$  and  $A$  being convex, we have  $A'(t) > -1$  and the denominator in both (12) and (13) is well-defined. Moreover,  $A'(t) \leq 1$ , otherwise we would have  $A(1 - \epsilon) < 1 - \epsilon$  for a sufficiently small  $\epsilon$ . Therefore,  $W'(x) \leq x$  for all  $x \in (0, 1)$ . On the other hand, the convexity of  $W$  follows directly from  $A''(t) \geq 0$ .  $\square$

**Remark 1.** *We do not need the smoothness assumption in Proposition 1 in either direction. We can argue that affine transformations map convex epigraphs into convex epigraphs<sup>2</sup>. Hence, the convexity of  $A$  is equivalent to that of  $W$ . Nonetheless, differentiability is a convenient requirement for our construction.*

Let us analyze how some properties of  $A$  translate into  $W$ .

**Proposition 2.** *Let  $A$  and  $W$  be like in Proposition 1.*

1.  *$A$  is symmetrical, i.e.,  $A(t) = A(1 - t)$  for all  $t \in [0, 1]$ , iff  $W$  is invertible and  $W^{-1} = W$ .*
2.  *$W$  has a unique fixed point  $x^* = x(1/2) = A(1/2) - 1/2$ .*
3. *If  $W$  is twice differentiable with  $W''(x) > 0$ , for all  $x \in (0, 1)$ , and satisfies  $W^{-1} = W$ , then  $W'(x) = -1$  iff  $x = x^*$ , the fixed point.*

*Proof.* Let us suppose  $A$  is symmetrical. First,  $W$  must be one-to-one, since  $W(x_1) = W(x_2)$  for some  $x_1, x_2 \in [0, 1]$ ,  $x_1 < x_2$ , would imply,  $W$  being non-increasing, that  $W$  is constant over  $[x_1, x_2]$ . Using (9), we get that  $A(t) - t$  is constant over  $t \in [t_1, t_2] \equiv [t(x_1), t(x_2)]$ . That means  $A(t) = a + t$  over  $[t_1, t_2]$ , for some constant  $a \in \mathbb{R}$ . What is more, since  $A(t) > 1 - t$  and  $A$  is symmetrical, it turns out that  $A(t) > t$  for all  $t \in (0, 1)$ , thus  $a >$

<sup>2</sup>Recall that a function is convex iff its epigraph is a convex set.

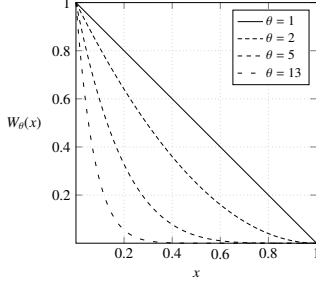


Figure 4: Different instances of the 2-monotone family  $W_\theta(x) = (1-x)^\theta$ .

0 necessarily. Now, form the line segment  $S(t)$ , for  $t \in [t_1, 1]$ , that satisfies  $S(t_1) = A(t_1) = a + t_1$  and  $S(1) = A(1) = 1$ . It is easy to check that the slope of such an  $S$  is  $s = (1-a-t_1)/(1-t_1)$  and satisfies  $0 < s < 1$ . Then,  $S(t_2) = a + t_1 + s(t_2 - t_1) < a + t_2 = A(t_2)$ , which contradicts the convexity of  $A$ . Therefore,  $W$  is one-to-one and has inverse  $W^{-1}$ .

Next, to see  $W^{-1} = W$ , let us start by noting in (9) that the symmetry of  $A$  leads to  $x(1-t) = W(x(t))$ . Then, applying  $W$  to the right side in the latter equation and using it again with argument  $1-t$ , we get  $W(W(x(t))) = W(x(1-t)) = x(t)$ . Because  $x(t)$  is an automorphism, we have  $W(W(x)) = x$ , for all  $x \in [0, 1]$ .

Conversely, suppose  $W^{-1} = W$ . Using  $W(W(x)) = x$ , straight calculations lead to both  $t(W(x)) = 1 - t(x)$  and  $A(t(W(x))) = A(t(x))$  and, hence,  $A(1 - t(x)) = A(t(x))$ , for all  $x \in [0, 1]$ , so  $A$  is symmetrical.

For the second part of the proposition, just note that  $W(x(t)) = x(t)$  iff  $t = 1/2$ . Then, substituting  $t = 1/2$  in  $x(t)$  yields the expected result.

Finally, for the third part, it is clear that there must exist  $\tilde{x}$  such that  $W'(\tilde{x}) = -1$ . Moreover, as  $W''' > 0$ , that point must also be unique. Now, since  $W^{-1} = W$ , the corresponding  $A$  is symmetrical. Taking derivatives,  $A'(t) = -A'(1-t) = 0$  iff  $t = 1/2$ . Plugging it into (12), we get  $W'(x(1/2)) = -1$ , so  $\tilde{x} = x(1/2)$ , the fixed point from the second part.  $\square$

**Example 2.** Elaborating on Example 1, plugging  $A(t) = t^2 - t + 1$  into (9) yields the  $W(x) = x - 2\sqrt{x} + 1$  we see in Figure 3.

**Example 3.** The family of functions  $W_\theta(x) = (1-x)^\theta$ , where  $\theta \in [1, \infty)$ , meet the conditions in Proposition 1 and thus produce EVCs. Clearly, except for  $\theta = 1$ ,  $W_\theta^{-1} \neq W_\theta$  and, by Proposition 2, none of them produces an exchangeable EVC.

A  $W$  function like the one defined in Proposition 1 induces a spectral measure (2) by means of

$$\eta(z) = \frac{4 W'''(t^{-1}(z))}{[1 - W'(t^{-1}(z))]^3} \quad (14)$$

and

$$\mathcal{H}_0 = \frac{2}{1 - W'(0^+)}, \quad \mathcal{H}_1 = \frac{-2W'(1^-)}{1 - W'(1^-)}. \quad (15)$$

Such a  $W$  fails to attain the comonotonic copula, which has PF  $A(t) = \max\{1-t, t\}$ . However, it can still model independence if  $W(x) = 1-x$ .

### 3.1.2. Williamson's transform

Using  $W$  instead of  $A$  comes at practically no cost, but it still poses stringent constraints on derivatives and boundary conditions. We can solve the problem by taking  $W$  to be the Williamson transform (WT) of a random variable (rv) supported on  $[0, 1]$  that places no mass at 0.

Williamson's transform came into play in the context of ACs as a less restrictive integral transform than Laplace's. McNeil and Nešlehová [3] describe a connection between  $d$ -variate ACs and  $d$ -monotone functions obtained as Williamson  $d$ -transforms of non-negative rvs. Here we will restrict ourselves to the case  $d = 2$ .

**Definition 1.** [Williamson's transform] Let  $F$  be the CDF of a non-negative rv satisfying  $F(0) = 0$ . We define the WT of  $F$  as

$$\mathfrak{B}\{F\}(x) = \int_x^\infty \left(1 - \frac{x}{r}\right) dF(r).$$

A fundamental result in [3] states that  $\Psi = \mathfrak{B}\{F\}$  iff  $\Psi$  is 2-monotone and satisfies the boundary conditions  $\Psi(0) = 1$  and  $\Psi(\infty) = \lim_{x \rightarrow \infty} \Psi(x) = 0$ . Moreover, such an  $F$  is unique and can be retrieved from  $\Psi$  as  $F(x) = 1 - \Psi(x) + x \Psi'(x^+)$ .

It can be easily checked that the support of  $F$  is  $[0, x^*]$ , where  $x^* = \inf\{x \in \mathbb{R} \cup \{\infty\} \mid \Psi(x) = 0\}$ . In our case, contrary to [3, 5], the support is bounded, since  $W(1) = 0$ . Therefore, we get the following corollary.

**Corollary 1.** A function  $W : [0, 1] \rightarrow \mathbb{R}$  is 2-monotone<sup>3</sup> with  $W(0) = 1$  and  $W(1) = 0$  iff it can be expressed as

$$W(x) = \int_x^1 \left(1 - \frac{x}{r}\right) dF(r),$$

for some unique CDF  $F$  supported on  $[0, 1]$  and such that  $F(0) = 0$ .

Corollary 1 provides a full characterization of functions  $W$  in Proposition 1, smoothness assumptions apart, in terms of a much more manageable  $F$ , at the cost of an additional integration step. Recall, however, that  $W$  and  $F$  are equivalent. We can further simplify the construction of  $W$  by imposing  $F$  to be absolutely continuous with probability density function (pdf)  $f$ :

$$W(x) = \int_x^1 \left(1 - \frac{x}{r}\right) f(r) dr. \quad (17)$$

The form (17) adds smoothness to  $W$ . Differentiating (17) we get

<sup>3</sup>Non-negative, non-increasing and convex.

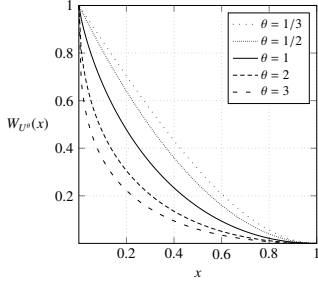


Figure 5: Different instances of the 2-monotone family (21). Values  $\theta < 1$  produce finite slopes at  $0^+$ . The case  $\theta = 2$  yields  $W_{U^2}(x) = x - 2\sqrt{x} + 1$ , the only member of the family that is its own inverse. The case  $\theta = 1/2$  coincides with the case  $\theta = 2$  in Figure 4 and Example 5.

$$W'(x) = - \int_x^1 \frac{f(r)}{r} dr, \quad W''(x) = \frac{f(x)}{x}. \quad (19)$$

All in all, the  $W$  function satisfies the equation

$$W(x) = \hat{F}(x) + x W'(x), \quad (20)$$

where  $\hat{F}(x) = 1 - F(x) = \int_x^1 f$  is the survival function of  $F$ . Equation (20) is useful for computational purposes.

From (18), it directly follows  $W'(1^-) = 0$ , thus  $\mathcal{H}_1$  in (16) is equal to zero. This feature prevents our method from reaching the independence copula, for which  $W(x) = 1 - x$ . The value of  $W'(0^+)$  (and subsequently of  $\mathcal{H}_0$ ) is, however, dependant on the behaviour of  $f$  near 0.

**Example 4.** Expanding on Example 2, by using (19), we find that  $F(x) = \sqrt{x}$ . Hence,  $F$  is the CDF of  $U^2$ , where  $U \sim \text{Unif}[0, 1]$ .

**Example 5.** Elaborating on Example 3, if  $\theta > 1$ , by (19), we get  $f(x) = \theta(\theta - 1)x(1 - x)^{\theta-2}$ , which is the pdf of the Beta( $\alpha = 2, \beta = \theta - 1$ ) distribution.

**Example 6.** Example 4 is a special case of WTs of positive<sup>4</sup> powers  $U^\theta$  of the uniform distribution on  $[0, 1]$ . The general formulas for their densities and CDFs are  $f_{U^\theta}(x) = \frac{1}{\theta}x^{\theta-1}$  and  $F_{U^\theta}(x) = x^{\frac{1}{\theta}}$ , respectively, whereas their WTs are given by

$$W_{U^\theta}(x) = \begin{cases} 1 + \frac{1}{\theta-1}x - \frac{\theta}{\theta-1}x^{\frac{1}{\theta}}, & \text{if } \theta \neq 1 \\ 1 - x + x \log x, & \text{if } \theta = 1 \end{cases}. \quad (21)$$

Figure 5 shows several instances of this family.

At this point, any  $n$ -parameter univariate pdf family  $\{f_\theta \mid \theta \in \mathbb{R}^n\}$  yields an equivalent  $n$ -parameter EVC family by integrating (17) and affinely transforming (8). However, the final target of our method are semiparametric models, where  $n$  can become arbitrarily large. We need to introduce further simplification and additional approximation techniques to produce such models.

<sup>4</sup>For  $\theta \leq 0$ , the resulting rv is not bounded.

### 3.1.3. Bayes space

For modelling  $f$ , we will turn to the Hilbert space of probability density functions [24, 25]. Consider the set  $\mathcal{P}$  of all pdfs  $f$  supported on  $[0, 1]$ , i.e., non-negative functions with  $\int_0^1 f = 1$ , and such that there exist  $m$  and  $M$  satisfying  $0 < m \leq f(x) < M$  for all  $x \in [0, 1]$ . Then, letting  $f, g \in \mathcal{P}$  and  $\alpha \in \mathbb{R}$ , consider the addition and scalar multiplication operations

$$(f \oplus g)(x) = \frac{f(x)g(x)}{\int_0^1 f(y)g(y) dy}, \quad (\alpha \odot f)(x) = \frac{f(x)^\alpha}{\int_0^1 f(y)^\alpha dy}.$$

Finally, consider the inner product

$$\langle f, g \rangle_{\mathcal{B}^2} = \frac{1}{2} \int_{[0,1]^2} \log \frac{f(x)}{f(y)} \log \frac{g(x)}{g(y)} dx dy.$$

Endowed with all these elements and after completion,  $\mathcal{B}^2 = (\mathcal{P}, \oplus, \odot, \langle, \rangle)$  is the Hilbert space [24] of square-integrable logarithm, where the null element corresponds to the uniform density,  $\text{Unif}[0, 1]$ . This construction is the continuous counterpart of Aitchison geometry [24].

In what follows, we shall use the above operations indistinctly with pdfs, distributions or rvs.

The space  $\mathcal{B}^2$  can be injected into  $L^2([0, 1])$  employing the centred log-ratio (CLR) transformation

$$\text{clr}[f](x) = \log f(x) - \int_0^1 \log f(y) dy. \quad (22)$$

However, note that not every element in  $L^2([0, 1])$  is attainable, since (22) introduces the constraint  $\int_0^1 \text{clr}[f] = 0$ . If we define the subspace  $L_0^2([0, 1])$  of the functions with zero integral, then (22) is a bijection from  $\mathcal{B}^2$  to  $L_0^2([0, 1])$  with inverse

$$\text{clr}^{-1}[p](x) = \frac{\exp p(x)}{\int_0^1 \exp p(y) dy}. \quad (23)$$

What is more, (22) is an isometry between  $\mathcal{B}^2$  and  $L_0^2([0, 1])$ .

**Example 7.** The densities of positive powers  $U^\theta$  of the uniform distribution in Example 6 have CLR transforms  $\text{clr}[U^\theta](x) = \frac{1-\theta}{\theta}(1 + \log x)$ . It immediately follows that all  $U^\theta$  are linearly dependent.

**Example 8.** The mirrored version  $1 - U^\theta$  of Example 6 can also be considered, but this time its WT has no simple closed form. Notwithstanding, we can check that Beta( $\alpha, \beta$ ) =  $U^{\frac{1}{\alpha}} \oplus (1 - U^{\frac{1}{\beta}})$ , for  $\alpha, \beta \in (0, \infty)$ . All Beta distributions can be expressed in the CLR space as  $\lambda_1 \log ex + \lambda_2 \log e(1 - x)$ , for some  $\lambda_1, \lambda_2 \in \mathbb{R}$ .

Utilizing the isometry (23), we can search for a suitable function in  $L_0^2([0, 1])$ , where the usual notions of sum, scalar multiplication and inner product stand, and then transform it back to a pdf. However, this space is infinite-dimensional, thus in practice, we shall work on a finite subspace. Example 8 provides a premier example of a 2-dimensional subspace. In general, we will build a pdf  $f_\theta$  as a linear combination

$$f_\theta(x) = \bigoplus_{i=1}^n (\theta_i \odot \text{clr}^{-1}[\varphi_i])(x) = \text{clr}^{-1} \left[ \sum_{i=1}^n \theta_i \varphi_i(x) \right], \quad (24)$$

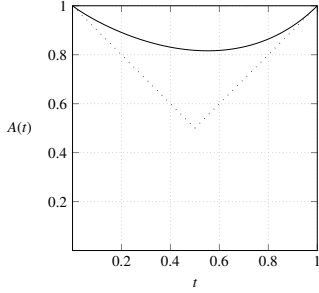


Figure 6: PF  $A(t) = 1 - t + \exp\{\mathcal{W}_{-1}(-2t/e^2) + 2\}$  arising from the Williamson family (21) for  $\theta = 1$ . Here,  $\mathcal{W}_{-1}$  denotes the  $k = -1$  branch of the complex Lambert W function.

where we can assume the  $(\varphi_i)_{i=1}^n$  are orthonormal, i.e.,  $\langle \varphi_i, \varphi_j \rangle_{L^2([0,1])} = \delta_{ij}$ , the Kronecker delta, and satisfy the zero-integral constraint.

The null element  $f_0 \sim \text{Unif}[0, 1]$  produces the WT (21) for  $\theta = 1$ . The resulting PF after rotation (8) has an explicit form that involves the Lambert W function [26]. Should the parameters in (24) be normally distributed with zero mean vector, we would expect the PF to lie close to the graph in Figure 6. In this sense, our method presents a very slight bias towards asymmetry.

The asymmetry bias can be corrected if we consider an affine subspace instead of a pure vector space, using a convenient  $\omega \in L^2([0, 1])$  as centre:

$$f_\theta = \text{clr}^{-1}[\omega] \oplus \bigoplus_{i=1}^n (\theta_i \odot \text{clr}^{-1}[\varphi_i]). \quad (25)$$

### 3.1.4. Compositional splines

Machalová et al. in [25] formalize the construction of a compliant zero-integral B-spline (ZBS) as a linear combination of the usual B-splines. We shall approximate the CLR space with the ZBS subspace. We refer the reader to [25] for further details on how to compute ZBSs and to [27] for more profound knowledge on B-splines, in general.

Splines are bounded functions. Committing to them, we would definitely have  $W'(0^+) = -\infty$  and thus  $\mathcal{H}_0 = 0$  in (15). Therefore, the resulting spectral measure would be absolutely continuous with respect to the Lebesgue measure on  $[0, 1]$  with Radon-Nikodym derivative equal to (14).

Given  $0 = \kappa_0 < \kappa_1 < \dots < \kappa_{n+1} = 1$ , where  $n \geq 0$ , and assuming  $2d$  additional coincidental<sup>5</sup> knots  $\kappa_{-d} = \dots = \kappa_{-1} = 0$  and  $\kappa_{n+2} = \dots = \kappa_{n+d+1} = 1$  at the endpoints, the space of splines  $p \in \mathcal{Z}_\kappa^d$  of degree less than or equal to  $d$  and  $n+2$  different knots  $\kappa = (\kappa_i)_{i=0}^{n+1}$  has dimension  $n+d$ . The case  $n=0$  corresponds to zero-integral polynomials over  $[0, 1]$ . Altogether, any zero-integral spline can be expressed as

$$p_\theta(x) = \sum_{i=1}^{n+d} \theta_i Z_i(x), \text{ for } \theta = (\theta_1, \dots, \theta_{n+d}) \in \mathbb{R}^{n+d}, \quad (26)$$

<sup>5</sup>Coincidental knots at the interval endpoints convey maximum smoothness at each interior knot [27]. For splines of degree less than or equal to  $d$ , we have  $(d-1)$ -continuous differentiability everywhere in  $[0, 1]$ .

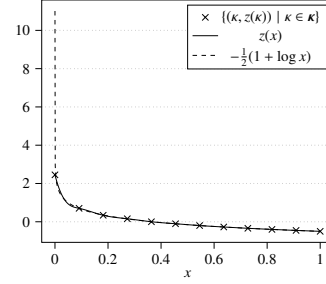


Figure 7: Projection  $z(x)$  of  $-\frac{1}{2}(1 + \log x)$  onto an orthonormal ZBS 13-dimensional basis with knots  $\kappa$ . The logarithmic function diverges to infinity at 0.

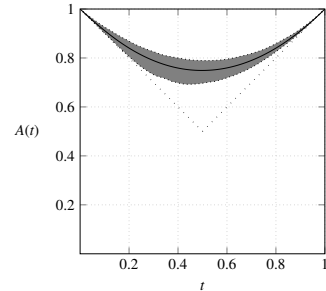


Figure 8: Random PFs built as perturbations around centre (27). Namely, all  $\theta_i$  were sampled from a normal distribution with zero mean and  $\sigma = 0.1$ . We randomly drew a total of 1,000 PFs. The solid line represents the mean function, while the grey envelope represents the confidence interval between quantiles 1% and 99%. The mean line is close to the  $A(t) = t^2 - t + 1$  in Figure 1.

where  $\int_0^1 Z_i = 0$  and we can further assume an orthonormal basis [25], i.e.,  $\langle Z_i, Z_j \rangle_{L^2} = \delta_{ij}$ . As  $\mathcal{Z}_\kappa^d \simeq \mathbb{R}^{n+d}$ , given  $p_{\theta_1}, p_{\theta_2} \in \mathcal{Z}_\kappa^d$ , we have  $\langle p_{\theta_1}, p_{\theta_2} \rangle_{L^2} = \langle \theta_1, \theta_2 \rangle_{\mathbb{R}^{n+d}} = \theta_1 \cdot \theta_2$ , the canonical dot product.

Furthermore, we can place a convenient centre for our ZBS space, so that the asymmetry bias is corrected. We propose to take  $\omega$  in (25) to be the orthogonal projection  $z$  of  $-\frac{1}{2}(1 + \log x)$ , the case  $\theta = 2$  in Example 7, onto the space (26):

$$z(x) = \sum_{i=1}^{n+d} \langle \text{clr}[U^2], Z_i \rangle_{L^2} Z_i(x). \quad (27)$$

This way, the resulting zero-integral function remains a spline in the original basis, and coordinates may be updated by simply adding at each component the correspondent  $\langle \text{clr}[U^2], Z_i \rangle_{L^2}$  projection. Figure 7 shows that the logarithmic centre can be effectively approximated by a spline, despite the divergence near zero. Figure 8 shows the effectiveness of the bias correction. Figure 9 depicts the underlying orthonormal ZBS basis  $\{Z_i\}$ .

From a practical standpoint, (26) can be directly used in an MCMC simulation [28] to draw samples from the corresponding distribution, since  $p_\theta = \log f_\theta + K$ , for some constant  $K \in \mathbb{R}$  that eventually cancels out.

### 3.2. Convergence

In this section, we will present some elementary results on how convergence on the Bayes space relates to convergence for the resulting EVCs through our method.

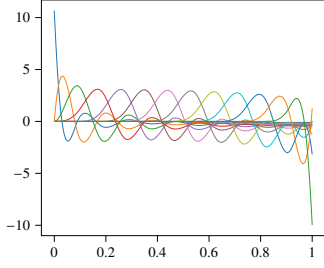


Figure 9: Orthonormal cubic ZBS basis with 13 elements.

We will use the supremum norm  $\|f\|_\infty = \sup_{x \in \mathcal{X}} |f(x)|$  of a bounded function  $f : \mathcal{X} \rightarrow \mathbb{R}$  to measure distances between some objects we have previously introduced.  $\mathcal{X}$  will typically be a compact subset of  $\mathbb{R}^n$ , namely  $[0, 1]$ , for functions  $W$  and  $A$ , and  $[0, 1]^2$ , for copulas  $C$ . The supremum norm defines a distance  $d_\infty(f, g) = \|f - g\|_\infty$ . A sequence of functions  $\{f_n\}_{n=1}^\infty$  converging on the latter distance to some  $f$  is said to converge *uniformly*.

Sometimes, however, uniform convergence is a relatively strong property to be realistically achieved. For instance, the function  $f$  may not be bounded on the whole  $\mathcal{X}$ . In those cases, a more subtle convergence exists, only requiring the sequence converging uniformly to  $f$  on every compact subset  $\mathcal{K}$  of  $\mathcal{X}$ . Then, the sequence of  $\{f_n\}_{n=1}^\infty$  is said to be *compactly convergent* to  $f$ .

The following related concept applies to probability measures.

**Definition 2.** Let  $\mathbb{P}$  and  $\mathbb{Q}$  be probability measures on the space  $[0, 1]$  equipped with the Borel  $\sigma$ -algebra  $\mathcal{B}$ . The *total variation distance (TVD)* between  $\mathbb{P}$  and  $\mathbb{Q}$  is defined as

$$d_{\text{TVD}}(\mathbb{P}, \mathbb{Q}) = \sup_{B \in \mathcal{B}} |\mathbb{P}(B) - \mathbb{Q}(B)|.$$

TVD satisfies all three axioms of a proper metric. By Scheffé's theorem [29], it can also be expressed in terms of the pdfs  $f$  and  $g$  of  $\mathbb{P}$  and  $\mathbb{Q}$ , respectively, as

$$d_{\text{TVD}}(\mathbb{P}, \mathbb{Q}) \equiv d_{\text{TVD}}(f, g) = \frac{1}{2} \int_0^1 |f(x) - g(x)| dx. \quad (28)$$

Our first result links convergence in TVD of a sequence of pdfs with convergence of the corresponding sequence of WTs and their derivatives.

**Proposition 3.** Let  $\{f_n\}_{n=1}^\infty$  be a sequence of pdfs supported on  $[0, 1]$  such that  $\lim_{n \rightarrow \infty} d_{\text{TVD}}(f, f_n) = 0$  for some pdf  $f$  also on  $[0, 1]$ . Let  $W_n$  and  $W$  be the corresponding Williamson transforms of  $f_n$  and  $f$ , respectively. Then, the sequence  $\{W_n\}_{n=1}^\infty$  uniformly converges to  $W$  on  $[0, 1]$ . Moreover,  $\{W'_n\}_{n=1}^\infty$  compactly converges to  $W'$  on  $(0, 1)$ .

*Proof.* It suffices to check that, for all  $x \in [0, 1]$ ,

$$\begin{aligned} |W(x) - W_n(x)| &= \left| \int_0^1 \left(1 - \frac{x}{r}\right)_+ [f(r) - f_n(r)] dr \right| \\ &\leq \int_0^1 |f(r) - f_n(r)| dr, \end{aligned}$$

where  $(\cdot)_+$  denotes the non-negative part of the argument, and then apply Scheffé's theorem (28). Similarly, considering the compact subset  $[x_0, 1]$ , for some  $x_0 > 0$ , we have, for all  $x \in [x_0, 1]$ ,  $|W'(x) - W'_n(x)| \leq \frac{2}{x_0} d_{\text{TVD}}(f, f_n)$ .  $\square$

The next step links the uniform convergence of WTs with that of PFs. Note, however, that uniform convergence of pointwise-convergent sequences of PFs can be established by other means, as pointed out in [30]. Nonetheless, the following result also states the uniform convergence of the first derivatives of PFs under the same hypotheses, which cannot be taken for granted.

**Proposition 4.** Let  $\{W_n\}_{n=1}^\infty$  be a sequence of WTs, arising from pdfs, uniformly convergent to some other WT  $W$  on  $[0, 1]$ . Also, suppose the sequence of first derivatives  $\{W'_n\}_{n=1}^\infty$  of the previous functions compactly converge to  $W'$  on  $(0, 1)$ . Let  $A_n$  and  $A$  be the corresponding PFs of  $W_n$  and  $W$ , respectively, according to our method. Then, the sequence  $\{A_n\}_{n=1}^\infty$  uniformly converges to  $A$  on  $[0, 1]$ , while  $\{A'_n\}_{n=1}^\infty$  compactly converges to  $A'$  on  $(0, 1)$ .

*Proof.* It follows from the equivalence between uniform convergence and function graph convergence [31] for functions with compact domain and range. Since the  $W_n$ 's uniformly converge to a continuous function  $W$ , the sequence of the graphs of the  $W_n$ 's has its limit in the graph of  $W$ . Then, note that the graphs of  $A_n$  and  $A$  are *affine transformations* (8) of the graphs of  $W_n$  and  $W$ , respectively. This ensures, by continuity, that the graphs of the  $A_n$ 's tend to that of  $A$ . Finally, graph convergence for the  $A_n$ 's implies uniform convergence to  $A$  itself.

The result for the first derivatives follows similarly. Instead of an affine map, the functions mapping the graph of  $W$  to that of  $A$  and vice versa are, respectively,

$$\mathbb{T}(x, w') = \left[ t(x), \frac{1+w'}{1-w'} \right], \quad \mathbb{X}(t, a') = \left[ x(t), \frac{a'-1}{a'+1} \right].$$

Both are the inverse of one another because of (10) and (12). Both functions are continuous. Hence, they preserve compactness and graph convergence.

To see that  $\{A'_n\}_{n=1}^\infty$  compactly converges to  $A'$ , consider any compact set  $\mathcal{K} = [t_0, 1]$ , for  $t_0 > 0$ . Then, consider the sequence of restricted function graphs  $\{\mathcal{G}[A'_n|_{\mathcal{K}}]\}_{n=1}^\infty$  and apply  $\mathbb{X}$  to every element to obtain another sequence  $\{\mathcal{G}[W'_n|_{\mathbb{X}(\mathcal{K})}]\}_{n=1}^\infty$ . Now,  $\mathbb{X}(\mathcal{K})$  is a compact set, so  $W'_n|_{\mathbb{X}(\mathcal{K})}$  uniformly converges to  $W'|_{\mathbb{X}(\mathcal{K})}$  and, because of [31], the graph sequence approaches  $\mathcal{G}[W'|_{\mathbb{X}(\mathcal{K})}]$ . The argument finishes by noting that, since  $\mathbb{T}$  is continuous and since  $\mathbb{T}(\mathcal{G}[W'_n|_{\mathbb{X}(\mathcal{K})}]) = \mathcal{G}[A'_n|_{\mathcal{K}}]$  and  $\mathbb{T}(\mathcal{G}[W'|_{\mathbb{X}(\mathcal{K})}]) = \mathcal{G}[A'|_{\mathcal{K}}]$ , the graphs of the  $A'_n|_{\mathcal{K}}$ 's tend to that of  $A'|_{\mathcal{K}}$ .  $\square$

**Remark 2.** Uniform convergence of function derivatives is mainly unconnected to uniform convergence of the functions themselves. The reason why it works, in this case, comes down to Williamson's transform, whose first derivative is also in a convenient integral form that allows applying TVD convergence of the internal pdfs to both the function and its derivative simultaneously.



Some topological arguments allow establishing uniform convergence of copulas from pointwise convergence alone [32]. Notwithstanding, there exists a connection between the supremum norms of copulas and those of their respective PFs [8]. Namely,  $\|C_1 - C_2\|_\infty \leq 2\gamma/(1+2\gamma)^{1+1/(2\gamma)}$ , where  $\gamma = \|A_1 - A_2\|_\infty$ .

We turn next to some assumptions making convergence in  $L_0^2([0, 1])$  sufficient for pdfs to converge in TVD.

**Proposition 5.** *Let  $\{p_n\}_{n=1}^\infty \subset L_0^2([0, 1])$  continuous and uniformly bounded, i.e.,  $\|p_n\|_\infty \leq K$  for some  $K > 0$  and for all  $n$ . Suppose  $\lim_{n \rightarrow \infty} \|p - p_n\|_2 = 0$ , for some  $p \in L_0^2([0, 1])$ . Let  $f_n = \text{clr}^{-1}[p_n]$  and  $f = \text{clr}^{-1}[p]$ . Then,  $\lim_{n \rightarrow \infty} d_{\text{TVD}}(f, f_n) = 0$ .*

*Proof.* First, note that continuity ensures that the limit  $p$  is also bounded by the same  $K$ . Denoting  $I_q = \int_0^1 e^q$ , some easy calculations show that

$$|f(x) - f_n(x)| \leq \frac{e^{p(x)}|I_p - I_{p_n}| + I_p |e^{p(x)} - e^{p_n(x)}|}{I_p I_{p_n}}.$$

Now, the integrals are bounded, namely  $e^{-K} \leq I_q \leq e^K$ . On the other hand,  $|e^{p(x)} - e^{p_n(x)}| \leq e^K |p(x) - p_n(x)|$ , using the *mean value theorem* and the fact that both functions are bounded by  $K$ . All in all,

$$|f(x) - f_n(x)| \leq e^{4K} \left( \int_0^1 |p(y) - p_n(y)| dy + |p(x) - p_n(x)| \right).$$

Integrating both sides of the last inequality and using Jensen's inequality, we finally get  $d_{\text{TVD}}(f, f_n) \leq e^{4K} \|p - p_n\|_2$ .  $\square$

Our method, acting on convergent sequences in  $L_0^2([0, 1])$ , produces EVCs that not only uniformly converge but also whose partial derivatives do.

**Corollary 2.** *Let  $\{z_n\}_{n=1}^\infty \subset L_0^2([0, 1])$  be a sequence of uniformly bounded smooth cubic ZBSs that converge in the  $\|\cdot\|_2$  norm. The corresponding EVCs from our method  $\{C_n\}_{n=1}^\infty$  uniformly converge to some EVC  $C$ , satisfying, for  $i = 1, 2$ ,  $\partial_i C_n \xrightarrow[n \rightarrow \infty]{\|\cdot\|_\infty} \partial_i C$  compactly over  $(0, 1)^2$ .*

*Proof.* It follows from all the previous convergence results and the form of the partial derivative of an EVC [7, 33], where all the terms uniformly converge on compact sets.  $\square$

### 3.3. Association measures

As mentioned earlier, in the case of an EVC, Kendall's tau and Spearman's rho take the form of integrals involving the PF [8]. The substitution of the PF by the equivalent WT form and a change of variables afterwards do not provide any meaningful insight into the latter's role. However, the apparent relation between WTs and Lorenz curves reveals a new path for measuring association.

The WT  $W$  of a PF  $A$  satisfies the definition of a Lorenz [23] curve  $L$  after the change of variable  $L(x) = W(1 - x)$ , for  $x \in [0, 1]$ . Lorenz curves appear in econometrics for assessing wealth inequality through the Gini coefficient (GC)  $G = 1 - 2 \int_0^1 L$ . The  $G$  index has a geometrical interpretation as the area

between  $L$  and  $x \mapsto x$  divided by the area under  $x \mapsto x$ , which is equal to  $1/2$ . The same interpretation applies to  $W$  and, since  $\int_0^1 W = \int_0^1 L$ , we have  $G = 1 - 2 \int_0^1 W$ . A value of  $G = 0$  means wealth is uniformly distributed (the  $p\%$  wealthiest proportion of the population accumulate  $p\%$  of the total wealth, for all  $p \in [0, 1]$ ), whereas  $G \lesssim 1$  means that nearly all wealth belongs to a tiny fraction of the population. In summary,  $G = 0$  represents perfect equality, while  $G = 1$  represents perfect inequality.

Now, in our context, a PF  $A$  is just the affine transformation of some  $W$ . Since affine transformations change areas by applying a constant factor, the latter cancels out in ratio measures, leaving them invariant. Therefore, the GC is the area between  $A$  and the upper bound line  $\{y = 1\}$  divided by the area between the support lines and the upper bound line. This argument leads to  $G = 4 \left( 1 - \int_0^1 A \right)$ . The value  $G = 1$  happens when  $A$  is identically equal to the lower support lines ( $\int_0^1 A = 3/4$ ), producing the comonotonic copula. On the other hand,  $G = 0$  occurs when  $A$  is identical to the upper bound line ( $\int_0^1 A = 1$ ), producing the independence copula. This way, the bivariate positive association can be interpreted in econometric terms: comonotonicity is equivalent to perfect inequality, whereas independence corresponds to perfect equality.

The GC is an uncommon association measure in the context of EVCs, despite its simplicity. We have only found a brief mention of a slightly modified version of it in [34], where the measure was not scaled to lie on  $[0, 1]$ . Moreover, PF symmetry was further assumed. The index can be reformulated for any *positively quadrant dependent* copula  $C$ , i.e.,  $C(u, v) \geq uv$ , for all  $u, v \in [0, 1]^2$ , as<sup>6</sup>

$$G = 4 \left( 1 - \int_{[0,1]^2} \frac{\log C(u, v)}{\log uv} dudv \right). \quad (29)$$

The GC, as defined above, satisfies the axioms of a *dependence measure* [2], taking values on  $[0, 1]$ , unlike Kendall's tau and Spearman's rho, which belong to a more general family of *concordance measures*, ranging in  $[-1, 1]$  and allowing for negative association. Although we call it the GC, because of its origin, it is not to be confused with another well-known concordance measure: Gini's gamma.

Interestingly, after integrating by parts twice, the area of  $W$  can be expressed in terms of the inner density  $f$ , yielding  $G = 1 - \mathbb{E}[X]$ , where  $X \sim f$ . The latter equation links a complex integral calculation in two dimensions (29) to a much simpler one, which can even be approximated by MCMC simulation only evaluating the underlying ZBS.

**Example 9.** The EVC family defined in Example 5 has a wide range of GC values, in terms of a parameter  $\theta \in [1, \infty)$ , as  $G = (\theta - 1)/(\theta + 1)$ .

**Example 10.** The EVC family defined in Example 6 also has a wide range of GC values, in terms of a parameter  $\theta \in (0, \infty)$ , as  $G = \theta/(\theta + 1)$ .

<sup>6</sup>The CDF (4) and its stochastic interpretation provide a shortcut to check this.

### 3.4. Estimation

The estimation process builds upon the various constructions explored above. Given an orthonormal ZBS basis, we aim to find the parameter vector  $\theta$  that best fits a dataset. Starting from a ZBS (24)  $p_\theta$ , we apply the inverse CLR transformation (23) to obtain a pdf  $f_\theta$  over  $[0, 1]$ . Then, we integrate the pdf using the WT (17) to obtain a 2-monotone function  $W_\theta$ . Finally, we rotate that function to get to the targeted PF  $A_\theta$ , using (8). Once arrived at the PF, the construction of the EVC follows from the definition (1).

Knowing the one-to-one relation [15] between the random vector  $(U, V)$  following an EVC and the rv  $Z = \log U / \log(UV)$ , we reduce our problem to fitting the latter, which has a simpler pdf, straightly derived from (4):

$$h(z) = 1 + (1 - 2z) \frac{A'(z)}{A(z)} + z(1 - z) \left[ \frac{A''(z)}{A(z)} - \left( \frac{A'(z)}{A(z)} \right)^2 \right]. \quad (30)$$

The corresponding  $\tilde{h}$  for the symmetrical counterpart  $\tilde{A}$  of  $A$  is  $z \mapsto h(1 - z)$ . Therefore,  $A$  will be symmetrical iff  $h$  is symmetrical around the  $\{z = 1/2\}$  axis.

Given a random sample  $\mathcal{D} = \{z_i\}_{i=1}^m$  from  $Z$  and a model  $h_\theta$  derived from  $p_\theta$  up to  $A_\theta$ , the frequentist approach to the estimation addresses the maximization of the penalized log-likelihood of  $h_\theta$

$$\ell(\theta|\mathcal{D}) = \sum_{i=1}^m \log h_\theta(z_i) - \lambda \int_0^1 (p_\theta''(x))^2 dx, \quad (31)$$

for some regularization hyper-parameter  $\lambda \geq 0$ . The square norm term involving  $p_\theta''$  is the linearized curvature of the spline: a simplified non-intrinsic form of the curvature that can be expressed as a covariant tensor  $\theta^T \Omega \theta$ , where  $\Omega = (\Omega_{ij}) = (\int_0^1 Z_i'' Z_j'')$ . Splines may exhibit complex shapes prone to overfitting, as shown in Figure (9). Penalizing the curvature is the proposed method in [25] in the context of compositional data regression. Hernández-Lobato and Suárez applied this approach in semiparametric copula models before [19]. Taking  $\lambda = 0$  removes regularization, retrieving the usual log-likelihood.

Estimating the parameters of such a model poses some important challenges. First and foremost, the evaluation alone of the resulting PF from a parameter vector and a single argument implies several non-trivial operations, most notably the integral and affine transformations (17) and (8), respectively. Although they can be accurately applied, from a numerical standpoint, they are time-consuming, which may hinder the overall estimation process. Therefore, we propose critical approximations at each step.

First, note that the evaluation of  $A$  in (8) at a specific value  $t_0$  requires solving for  $x$  in  $t(x) = t_0$ . The latter will generally be a nonlinear equation that can only be solved through numerical methods at a relatively high computational cost. Hence, in most cases, evaluating (30) in (31) at each point  $z_i$  becomes rapidly unaffordable as  $m$  increases. What is more, any root finding procedure of our choice would prevent us from applying gradient optimization, as it would stop backpropagation. Considering all, we propose to approximate  $h_\theta$  by a piecewise linear

interpolator  $\tilde{h}$  with sufficiently numerous and carefully selected knots.

Since (31) is based on an empirical univariate sample  $\mathcal{D}$ , a reasonable knot selection utilizes uniform quantiles of  $\mathcal{D}$ , thus knots will be more spaced on low probability regions and will accumulate on high probability ones. This criterion, which was employed in a similar setting in [19], reduces the variance of the parameter vector  $\theta$ . Once fixed the quantiles  $\{q_i\}_{i=1}^k$ , we need to estimate some  $\{x_i\}_{i=1}^k$  such that  $t_i \equiv t_\theta(x_i) \approx q_i$  and then take  $h_i = h_\theta(t_i)$  as the linear interpolator value at knot  $t_i$ . Note that the  $t_i$ 's are just approximations for the  $q_i$ 's. To estimate the required  $x_i$ 's, we may apply (9) over the  $q_i$ 's grid using an empirical nonparametric estimate of the PF, like (5). We can state the procedure as follows.

**Algorithm 1.** Let  $\mathcal{D} = \{z_i\}_{i=1}^m$  be a random sample following the  $H$  distribution. To build an interpolation grid  $\{x_i\}_{i=0}^{k+1}$  in the  $W$  space such that  $\{t(x_i)\}_{i=0}^{k+1}$  are roughly distributed according to  $\mathcal{D}$ , follow these steps:

1. Pick  $k$  uniform quantiles  $0 = q_0 < q_1 < \dots < q_{k+1} = 1$  of  $\mathcal{D}$ .
2. Build the empirical CDF  $\tilde{H}$  of  $\mathcal{D}$ .
3. Build an empirical estimate  $\tilde{A}$  using  $\tilde{H}$  and (5).
4. Ensure boundary constraints taking

$$\hat{A}(t) = \min\{1, \max\{t, 1 - t, \tilde{A}(t)\}\}.$$

5. Set  $x_0 = 0$  and  $x_{k+1} = 1$ . Then, for every  $i = 1, \dots, k$ , set  $x_i = q_i + \hat{A}(q_i) - 1$ .
6. Sort ascendingly the resulting  $\{x_i\}_{i=0}^{k+1}$  and remove duplicates if needed.

We can reuse the grid obtained in the last algorithm throughout the estimation process, at every gradient descent step and with different values for the parameter vector  $\theta$ . With this grid and with a parameter vector  $\theta$  we can now build a light version of  $h_\theta$  to evaluate the penalized log-likelihood. Early experiments also suggest that selecting spline knots for  $p_\theta$  according to Algorithm 1 is key to constructing an unbiased estimator  $A_\theta$ .

Along with the interpolation grid, we need to estimate the values of  $W_\theta$  and its derivatives from  $p_\theta$ .

**Algorithm 2.** Let  $p_\theta$  be the ZBS corresponding to the parameter vector  $\theta$ . Let  $\{r_i\}_{i=0}^{n+1}$  be a strictly increasing real sequence such that  $r_0 = 0$  and  $r_{n+1} = 1$ . Let  $\epsilon \gtrsim 0$  such that  $\epsilon < r_1$ . To build an approximation to the corresponding WT  $W_\theta$  and its first and second derivatives, follow these steps:

1. For  $i = 0, \dots, n + 1$ , set  $p_i = \exp p_\theta(r_i)$ .
2. Compute  $I \approx \int_0^1 \exp p_\theta$  using the composite trapezoidal rule over  $\{(r_i, p_i)\}_{i=0}^{n+1}$ .
3. For  $i = 0, \dots, n + 1$ , set  $f_i = p_i/I$ .
4. Set  $s_0 = \epsilon$ . Then, for  $i = 1, \dots, n + 1$ , set  $s_i = r_i$ .
5. For  $i = 0, \dots, n + 1$ , set  $\tilde{W}_i''' = f_i/s_i$ .
6. For  $i = 0, \dots, n$ , set  $\Delta_i = s_{i+1} - s_i$ .
7. For  $i = 0, \dots, n$ , set  $P_i = \Delta_i^{(f_i + f_{i+1})/2}$  and  $Q_i = \Delta_i^{(\tilde{W}_i''' + \tilde{W}_{i+1}''')/2}$ .

8. Set  $\bar{W}'_{n+1} = 0$ . Then, for  $i$  from  $n$  down to 0, compute  $\bar{W}'_i$  using the recurrence relation

$$\bar{W}'_i = \bar{W}'_{i+1} - Q_i. \quad (32)$$

9. For  $i = 0, \dots, n+1$ , set  $\delta_i = s_i \bar{W}'_i$ .  
 10. Set  $\bar{W}_{n+1} = 0$ . Then, for  $i$  from  $n$  down to 0, compute  $\bar{W}_i$  using the recurrence relation

$$\bar{W}_i = \bar{W}_{i+1} + \delta_i - \delta_{i+1} + P_i. \quad (33)$$

11. For  $i = 0, \dots, n+1$ , set  $W_i = \bar{W}_i / \bar{W}_0$ ,  $W'_i = \bar{W}'_i / \bar{W}_0$ ,  $W''_i = \bar{W}''_i / \bar{W}_0$ .  
 12. Build a piecewise linear interpolator  $\tilde{W}^0$  from  $\{(r_i, W_i)\}_{i=0}^{n+1}$  for  $W_\theta$ .  
 13. Build a piecewise linear interpolator  $\tilde{W}^1$  from  $\{(r_i, W'_i)\}_{i=0}^{n+1}$  for  $W'_\theta$ .  
 14. Build a piecewise linear interpolator  $\tilde{W}^2$  from  $\{(r_i, W''_i)\}_{i=0}^{n+1}$  for  $W''_\theta$ .

*Proof.* Let us set aside the normalization by  $\bar{W}_0$  for a moment. Clearly,  $\bar{W}''_i$  is a straight approximation for  $W''_\theta(r_i)$ . It only remains to check that (33) and (32) provide good approximations for  $W_\theta(r_i)$  and  $W'_\theta(r_i)$ , respectively. It suffices to see that

$$\bar{W}'_i = \sum_{j=i}^n \bar{W}'_j - \bar{W}'_{j+1} = - \sum_{j=i}^n Q_j \approx - \int_{r_i}^1 \frac{f_\theta(r)}{r} dr$$

and, taking into account (20),

$$\begin{aligned} \bar{W}_i &= \sum_{j=i}^n \bar{W}_j - \bar{W}_{j+1} = \sum_{j=i}^n s_j \bar{W}'_j - s_{j+1} \bar{W}'_{j+1} + P_j \\ &= s_i \bar{W}'_i + \sum_{j=i}^n P_j \approx r_i W'_\theta(r_i) + \int_{r_i}^1 f_\theta(r) dr, \end{aligned}$$

where we have used that  $P_i$  and  $Q_i$  are the trapezoidal rule approximations for  $\int_{r_i}^{r_{i+1}} f_\theta$  and  $\int_{r_i}^{r_{i+1}} f_\theta(r)/r dr$ , respectively. Also, implicit in the previous argument was the approximation  $s_0 = \epsilon \approx 0$ , used to avoid infinite values. Finally, the last normalization step aims to stabilize the estimation process against numerical errors, enforcing the constraint  $W_\theta(0) = 1$ .  $\square$

Now, we are ready to build a light version of  $h_\theta$ .

**Algorithm 3.** Let  $\{x_i\}_{i=0}^{k+1}$  be the interpolation grid from Algorithm 1. Let  $\tilde{W}^0$ ,  $\tilde{W}^1$  and  $\tilde{W}^2$  be the piecewise linear approximations to  $W_\theta$ ,  $W'_\theta$  and  $W''_\theta$  from Algorithm 2, respectively. To build an approximation for  $h_\theta$ , follow these steps:

1. For  $i = 1, \dots, k$ , set  $W_i = \tilde{W}^0(x_i)$ ,  $W'_i = \tilde{W}^1(x_i)$ ,  $W''_i = \tilde{W}^2(x_i)$ .
2. Set  $t_0 = 0$  and  $t_{k+1} = 1$ . Then, for  $i = 1, \dots, k$ , set  $t_i = (1+x_i-W_i)/2$ .
3. For  $i = 1, \dots, k$ , set  $A_i = (1+x_i+W_i)/2$ .
4. For  $i = 1, \dots, k$ , set  $M_i = 1 - W'_i$ .
5. For  $i = 1, \dots, k$ , set  $A'_i = (1+W''_i)/M_i$ .
6. For  $i = 1, \dots, k$ , set  $A''_i = 4W''_i/M_i^3$ .

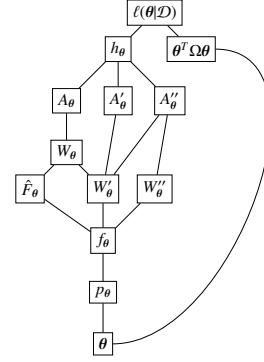


Figure 10: Computation graph for the estimation process, from the bottom parameter vector  $\theta$  up to the penalized log-likelihood  $\ell(\theta|\mathcal{D})$ .

7. For  $i = 1, \dots, k$ , set  $D_i = A'_i/A_i$ .
8. Set  $h_0 = h_{k+1} = 0$ . Then, for  $i = 1, \dots, k$ , set

$$h_i = 1 + (1 - 2t_i)D_i + t_i(1 - t_i) \left( \frac{A''_i}{A_i} - D_i^2 \right). \quad (34)$$

9. Build a piecewise linear interpolator  $\tilde{h}$  from  $\{(t_i, h_i)\}_{i=0}^{k+1}$ .
10. Compute  $I \approx \int_0^1 \tilde{h}$  using the composite trapezoidal rule over  $\{(t_i, h_i)\}_{i=0}^{k+1}$ .
11. Use  $\hat{h} = \tilde{h}/I$  as an approximation for  $h_\theta$  over  $[0, 1]$ .

*Proof.* The rationale of the algorithm is relatively straightforward. Equation (34) mimics (30), where  $A_\theta$  and its derivatives are evaluated over  $t_i$  indirectly through equations (8), (10) and (11), requiring only the  $x_i$ 's and approximations of  $W_\theta$  and its derivatives at those points. On the other hand, the reader can easily check that  $h_\theta(0) = h_\theta(1) = 0$ , considering all the constraints imposed by our method:  $A'_\theta(0^+) = -1$ ,  $A'_\theta(1^-) = 1$  and  $f_\theta(x) > 0$  for all  $x \in [0, 1]$ , among others. The case at the 0 endpoint is not trivial, but nearly so. After simplification, we arrive at

$$h_\theta(0) = 2f_\theta(0) \lim_{x \rightarrow 0^+} \frac{1+x-W_\theta(x)}{x(1-W'_\theta(x))^3}.$$

Repeatedly applying L'Hôpital's rule, we can check that the denominator tends to zero and, eventually, the whole limit also tends to zero. Finally, the step involving the integral ensures  $\int_0^1 \tilde{h} = 1$ , making a  $\tilde{h}$  a true pdf, which was not automatically granted by the linear interpolation strategy.  $\square$

Algorithm 3 deals with problems like the approximation of  $h_\theta$  and the rotation of  $W_\theta$ . On the other hand, Algorithm 2 formalizes an efficient computation scheme for  $W_\theta$ . Both together allow computing  $\ell(\theta|\mathcal{D})$ . Figure 10 shows the full computation graph. Gradients flow from the top penalized log-likelihood down the parameter vector using backpropagation. We recommend using the autograd package [35], capable of performing automatic differentiation on native Python operations. Some representative routines in our implementation are NumPy's `trapz`, for calculating integrals using the trapezoidal rule, and `cumsum`, for computing recurrences (32) and (33).

*Implementation tips.* Knowing  $W'_\theta(0^+) = -\infty$  and  $W''_\theta(0^+) = \infty$ , we recommend choosing the grid in Algorithm 2 so that points accumulate near zero, making the linear interpolation more effective. Chebyshev nodes are a standard option.

To adapt the estimation process to the particular hypotheses of our method, we propose to change the copula variable ordering whenever a steep slope is likely to appear for  $W_\theta$  near 0, which coincides with the minimum of  $A_\theta$  being placed at  $t < 0.5$ . We can heuristically assess this situation by calculating the mode of the pdf  $h$ , as suggested in [7]. If the mode is placed at  $t < 0.5$ , then the minimum of the PF is *likely* to be placed at  $t < 0.5$ . We support the hypothesis of [7] based on our own experience. Therefore, whenever the mode peaks at  $t < 0.5$ , we recommend changing the variable ordering before estimating and then flipping the resulting PF  $A$  as  $\tilde{A}(t) = A(1 - t)$ .

### 3.5. Simulation

Once the parameters  $\theta$  have been estimated, we propose to build  $W_\theta$  and  $A_\theta$  subsequently. From that point on, querying the model (simulating, estimating probabilities, among others) will be equivalent to evaluating the PF  $A_\theta$ , as with any other EVC.

The algorithms presented in Section 3.4 stand valid, with some minor and convenient changes. Since we only need to build the functions once, and not once per iteration, we may employ more expensive and accurate approximations. In particular,  $W''_\theta$  can be evaluated without approximations. Trapezoidal rules and linear interpolations should be replaced by more sophisticated procedures. On the other hand, Algorithm 1 is no longer required. Instead, we may employ a root-finding algorithm to invert the automorphism  $t$ .

The interpolation points of  $A_\theta$  could be input to the shape-preserving [36] interpolation procedure by Schumaker, which would guarantee that the resulting spline is convex over the whole domain. However, in general, the second derivative of such a spline would not be continuous, which would hinder the simulation process. In practice, for the intended use of this approximation, we recommend smoothness and accuracy over shape preservation.

Finally, to draw samples from  $C_\theta$ , we recommend the general algorithm in [2], which only requires inverting one of its partial derivatives [33, 7]. In this respect, the root-finding algorithm [37] proves to be extremely effective.

### 3.6. Refinement

One of the limitations of our method is the fact that an estimated PF  $A$  always satisfies  $A'(0^+) = -1$  and  $A'(1^-) = 1$ . These constraints are a consequence of our construction, which imposes  $W'(0^+) = -\infty$  and  $W'(1^-) = 0$  on the WT. In practice, however, these boundary constraints do not hinder the expressiveness of the resulting model. Remember that, for instance, upper tail dependence does not relate to either boundary derivative of the PF, but the mid-point value  $A(1/2)$ . This fact contrasts with the nature of another semiparametric procedure like [19], where a slope value entirely determined the tail index.

In our method, misspecified slopes for the PF have a much lower impact on the concordance (Blomqvist's beta) and upper tail dependence. Nonetheless, since it might produce a

slight bias, we propose a refinement step that could follow our method.

Khoudraji's method [10] is best known for inducing asymmetry in symmetrical EVCs. However, there is no reason why it could not apply to asymmetrical ones [11]. Consider a PF  $A$  obtained through our method. Differentiating (3) we arrive at

$$\begin{aligned} A'_{\alpha,\beta}(0^+) &= \beta A'(0^+) = -\beta \\ A'_{\alpha,\beta}(1^-) &= \alpha A'(1^-) = \alpha \end{aligned} \quad , \quad (35)$$

where, remember,  $\alpha, \beta \in (0, 1]$ , retrieving  $A$  for  $\alpha = \beta = 1$ . Even though  $A$  is, in general, asymmetrical, we see from (35) that Khoudraji's method serves our purpose of freely parameterizing the boundary slopes.<sup>7</sup>

We believe that adding two more parameters through Khoudraji's method may improve the fitness of the resulting model in some particular cases, especially for weak correlations. However, the inclusion of the new parameters in the gradient-based optimization seems unworkable, as it would invalidate the interpolation grid in Algorithm 3. A derivative-free optimization involving both the spline parameter vector  $\theta$  and the asymmetry parameters  $\alpha$  and  $\beta$  could be run, starting from  $\alpha = \beta = 1$  and some initial guess  $\theta = \theta_0$  obtained through a gradient-based method. In any case, the practical demonstration of such a procedure beyond theory is out of this paper's scope.

## 4. Results

In the following sections, we will test the proposed method (i) on simulated data and (ii) actual data.

### 4.1. Preliminaries

Before diving into the specific settings of each experiment, let us clarify some shared configuration aspects.

#### 4.1.1. Optimization

We performed all estimates using standard Python scientific packages like *NumPy* and *SciPy*, along with automatic differentiation, thanks to *autograd* [35]. Namely, we employed the *SciPy* implementation of the L-BFGS-B algorithm by Byrd et al. [38]. We assessed convergence by means of the `ftol=1e-6` configuration parameter in the `minimize` routine, which targets the relative change in the loss function between iterations. Even though this value is very conservative, the procedure converges well, with reasonable execution times, as we will see.

All estimation runs started at the null spline, with all coordinates equal to zero, regardless of using a fixed affine centre. Despite the caveats by Hernández-Lobato and Suárez [19], as was demonstrated in [39], current optimization methods are capable of dealing with complex problems even if the initial parameter values are far from the optimal solution. Notwithstanding, we agree with Hernández-Lobato and Suárez that good initial guesses would speed up the process even more.

<sup>7</sup>By convexity, the only EVC with either boundary slope equal to zero is the independence copula, with  $A(t) = 1$  for all  $t \in [0, 1]$ . Therefore, except for this limiting case, both slopes are allowed to vary freely.

#### 4.1.2. Resources

Both the SS and actual data application would not have been possible without the vast repertoire of software artefacts and services currently available.

First, our method, fully implemented in Python, was containerized using *Docker* [40], which, apart from being ideal for achieving reproducible research, also helped to move our execution environment to the cloud with *Kubernetes* [41].

While developing and testing, we employed a local *minikube* cluster [42] on an Intel® Core® i7-4700MQ CPU laptop with eight 2.40 GHz cores and equipped with 15.6 GiB of memory and operating system Ubuntu 20.04.3 LTS. We entrusted the bulky SS final executions to a cloud provider. The *Kubernetes* service comprised 50 dynamically allocated nodes running on possibly different<sup>8</sup> Intel® Xeon® architectures with Ubuntu 18.04. Overall, each node counted on two virtual CPUs and seven GiB of memory at any given time. Due to *Kubernetes*' requirements, only one CPU was available for *Spark* per node.

We sped up the experiments parallelizing specific tasks with *Spark* [43]. To prepare the *Spark* setting with *Kubernetes*, two artefacts were of great help: the *Docker image for Apache Spark* [44] and the *Spark Operator* [45].

Finally, *Argo CD* [46] turned out to be helpful to manage all our *Kubernetes* experiments from the same friendly user interface, connecting the *Kubernetes* cluster to the Git repository.

*Supplementary materials.* Access to source code and other deliverables will be provided upon acceptance for publication.

#### 4.2. Simulation study

We conducted a SS to test the effectiveness of our method on a broad spectrum of cases with high confidence. The SS consists of two independent experiments. The first one addresses the bias and variance tradeoffs by repeating the estimation process for many different random samples drawn from a fixed copula. On the other hand, the second experiment covers an even more extensive array of EVCs while focusing on validation through TVD.

Our method entails numerous non-trivial analytic and geometric transformations. Even though we could argue that none of them exceeds a reasonable level of complexity, clever algorithms and powerful computational resources are still needed for it to work in practice. In particular, optimization algorithms are vital to finding solutions that maximize (31) under memory and time constraints. The joint behaviour of all these pieces is difficult to assess from a purely theoretical perspective without simulations.

Despite the theoretical results presented in Section 3.2 and Section 3.3, which provide some interesting insights on the relation between the core pdf and the resulting EVC, the idea behind our construction is mainly pragmatic. Although a pdf is at the core of our construction, its stochastic properties cannot

be easily inferred from a sample other than through a full optimization run. This situation contrasts with nonparametric approaches like the one by Capéraà, Fougères, and Genest [15], where the asymptotic behaviour of the estimator could be theoretically established.

For all these reasons, simulations play a fundamental role in testing our method. Moreover, as will be seen in the second part, we resort to randomly generating PFs, using our construction, to produce a sufficiently varied benchmark set of EVCs.

*Common settings.* In both parts of the SS, copula models build upon a cubic orthonormal ZBS basis. The grid size was 200 both in Algorithm 2 and Algorithm 3 ( $n + 2 = 200$  and  $k + 2 = 200$ , respectively). Also, we took  $\epsilon = 10^{-9}$  in Algorithm 2. This settings express an adequate balance between approximation accuracy and reasonable execution times.

##### 4.2.1. Bias and variance

The first part of the study consisted of 30 individual experiments, each of them focusing on a particular instance of a copula family. For each copula instance, we performed an estimation run with our method on each of a set of 100 different random samples from the copula, for a combined total of 3,000 runs. Then, for each 100-sample experiment, we collected the pointwise means and pointwise 98% confidence intervals of the estimated PFs and compared both functional statistics with the original PF. We handled each random sample as an independent *Spark* task to speed up computations.

For this SS, we employed two of the families presented in Table 1: the Gumbel family and the Galambos family. These are probably two of the most well-known EVCs. Genest and Nešlehová even studied and found a relation between the two in [47], knowing the similarity of their PFs. In each copula family, we tested up to 5 different values of the unique parameter  $\theta$ , giving rise to different correlation levels. Finally, apart from the pure form of each Gumbel or Galambos copula, we introduced asymmetry by means of Khoudraji's device, taking either  $\alpha$  or  $\beta$  equal to 0.5 and leaving the other as 1. This configuration was precisely the one that demonstrated higher asymmetry in [48]. As a side note, we remind that the asymmetrical extensions of the Gumbel and Galambos families are known as the Tawn and Joe families, respectively.

Each of the random copula samples consisted of 1,000 observations. Our models were fit using 13 parameters in all cases: 10 more than the ground truth copula families. We believe that the specific number of parameters has less impact in a semiparametric context like this, where one typically employs a large number and then reduces overfitting by penalizing curvature. In the end, the target of this semiparametric method is a function, which lives in an infinite-dimensional space. In practice, both the Gumbel and the Galambos families need fewer parameters than 13, but in this case, we have preferred to stick to a large number to showcase the performance of the method in a general setting. Finally, for both the Gumbel and Galambos copulas, we used a curvature penalty factor  $\lambda = 10^{-5}$ .

Figure 11 shows the results for the Gumbel copulas, while Figure 12 presents those of the Galambos copulas. The results

<sup>8</sup>Either (i) Platinum 8272CL, (ii) 8171M 2.1GHz, (iii) E5-2673 v4 2.3 GHz or (iv) E5-2673 v3 2.4 GHz.

are qualitatively very similar. Our method displays low biases and variances in all cases. If any, the highest biases appear under asymmetry and low correlations. This behaviour matches the known limitation of our method as regards the boundary slopes, which have fixed values. Variance is also higher for small correlations, in agreement with [8].

In all simulations, we employed the trick mentioned in Section 3.4 for selecting the *a priori* more convenient variable ordering to avoid numerical instabilities. The procedure worked well, as demonstrated by the practically equal results obtained for either  $\alpha = 0.5$  or  $\beta = 0.5$ .

*Execution details.* We approximately recorded the execution times for the 30 experiments with the assistance of the Spark Web UI. Roughly 50% finished in three minutes, 75% in four and 90% in seven. The most time-consuming experiments, always below eight minutes, correspond to the highest correlated Gumbel and Galambos copulas. This is presumably because the optimal solution was furthest from the starting null vector. Considering that there were 100 tasks on each job and the cluster only had 50 nodes, we could expect the average execution time to be half of the previous values.

#### 4.2.2. Total variation

In the second part of the SS, we generated  $n = 200$  random EVCs by utilizing our construction method. We chose the affine spline model with centre (27) as the first building block, assuming uniformly distributed knots and a total of  $d = 13$  parameters. Let us call  $\theta_0 \in \mathbb{R}^d$  the coordinates of the centre of the affine model. We then ran an MCMC simulation assuming the model coordinates  $\theta$  in (25) were distributed according to the following pdf:

$$p(\theta) \propto \begin{cases} e^{-\lambda \bar{\theta}^T \Omega \bar{\theta}}, & \text{if } \|\theta\|_2 \leq R \\ 0, & \text{if } \|\theta\|_2 > R \end{cases}, \text{ for } \bar{\theta} = \theta + \theta_0,$$

where  $\Omega$  is the curvature matrix of the underlying spline, as described in Section 3.4, and  $\lambda$  and  $R$  are tuning parameters. The previous model is the truncated version of an improper prior based on curvature penalization, with factor  $\lambda$ . The support of the distribution is the hyperball of radius  $R$ .

We tuned the parameters with values  $\lambda = 10^{-4}$  and  $R = 5$  so that the resulting splines covered a wide range of correlations (in the sense of the GC) and were at the same time smooth. Finally, in order to prevent any asymmetry, we replaced the even elements in the sequence with their corresponding mirrored versions  $\tilde{A}(t) = A(1 - t)$ . Figure 13 shows a subsample of the generated random PFs. They cover the area between the support lines and the upper bound line in a reasonably balanced way. In this part of the SS, we also employed the heuristic to determine the most suitable variable ordering. Hence, we expected our method to perform well regardless of the orientation of the PF.

For each element in the sequence  $\{\theta_i\}_{i=1}^n$ , we built the EVC  $C_{\theta_i}$  and performed several estimation runs on random samples of different sizes  $\{S_j\}_{j=1}^m$ . All fitted models had the same number of parameters as the ground truth splines ( $d = 13$ ) and employed the same affine translation. The penalty factor in the

	mean	10%	25%	50%	75%	90%
sample size						
250	.06642	.0226	.03237	.04578	.06279	.08914
500	.04591	.01562	.02492	.03797	.05527	.07525
1000	.03701	.01333	.0213	.03093	.04301	.05994
2000	.0322	.01157	.01681	.02518	.03421	.05841

Table 2: Main summary statistics from the second part of the SS, mean and quantiles, for each sample size. TVD decreases as sample size increases.

loss function (31) was also set to  $\lambda = 10^{-4}$ . The only aspect in which estimated models differed from ground truth is spline knot placement, which was uniform for the latter, but empirically assessed for the former. Then, for each sample size  $S_j$ , we estimated a copula  $C_{ij}$  using our method and assessed divergence from ground truth through TVD

$$d_{\text{TVD}}(C_{\theta_i}, C_{ij}) = \frac{1}{2} \int_{[0,1]^2} |c_{\theta_i}(u, v) - c_{ij}(u, v)| \, dudv, \quad (36)$$

where  $c_{\theta_i}$  and  $c_{ij}$  are the pdfs of  $C_{\theta_i}$  and  $C_{ij}$ , respectively. The TVD defined in (36) is the bivariate counterpart of Definition 2 and thus provides an upper bound on the difference between the measured values of each copula on any measurable set  $B \subset [0, 1]^2$ . Therefore, (36) is a very conservative evaluation measure.

Table 2 presents the main summary statistics from the experiment. Each *Spark* task targeted a different random EVC. Then, each task comprised four estimation runs. The table shows promising results, considering the complexity of the ground truth models and the finiteness of samples. Mean values are typically below 0.05, whereas the 75% and 90% quantiles do not surpass the 0.10 threshold. Table 2 shows that TVD decreases as the sample size increases. Figure 14 reveals some outliers, which become rarer with larger sample sizes. Besides, Figure 14 suggests our method can generally handle well even the highest correlated samples.

The estimation algorithms are not entirely free of numerical instabilities that can trap the optimization process. However, most of these outliers are due to the sensitivity of the TVD metric to deviations in highly correlated samples. As Figure 15 shows, the TVD metric positively correlates with the GC even for moderate values of the latter, where the assumptions of our method are not compromised, and numerical errors should occur less often.

*Execution details.* The total execution time for the 200 random EVCs was roughly one hour. Considering the cluster only had 50 nodes, the average execution time for a task in this experiment was approximately 15 minutes.

#### 4.3. Real data applications

We will next present some results of our method on non-simulated data.

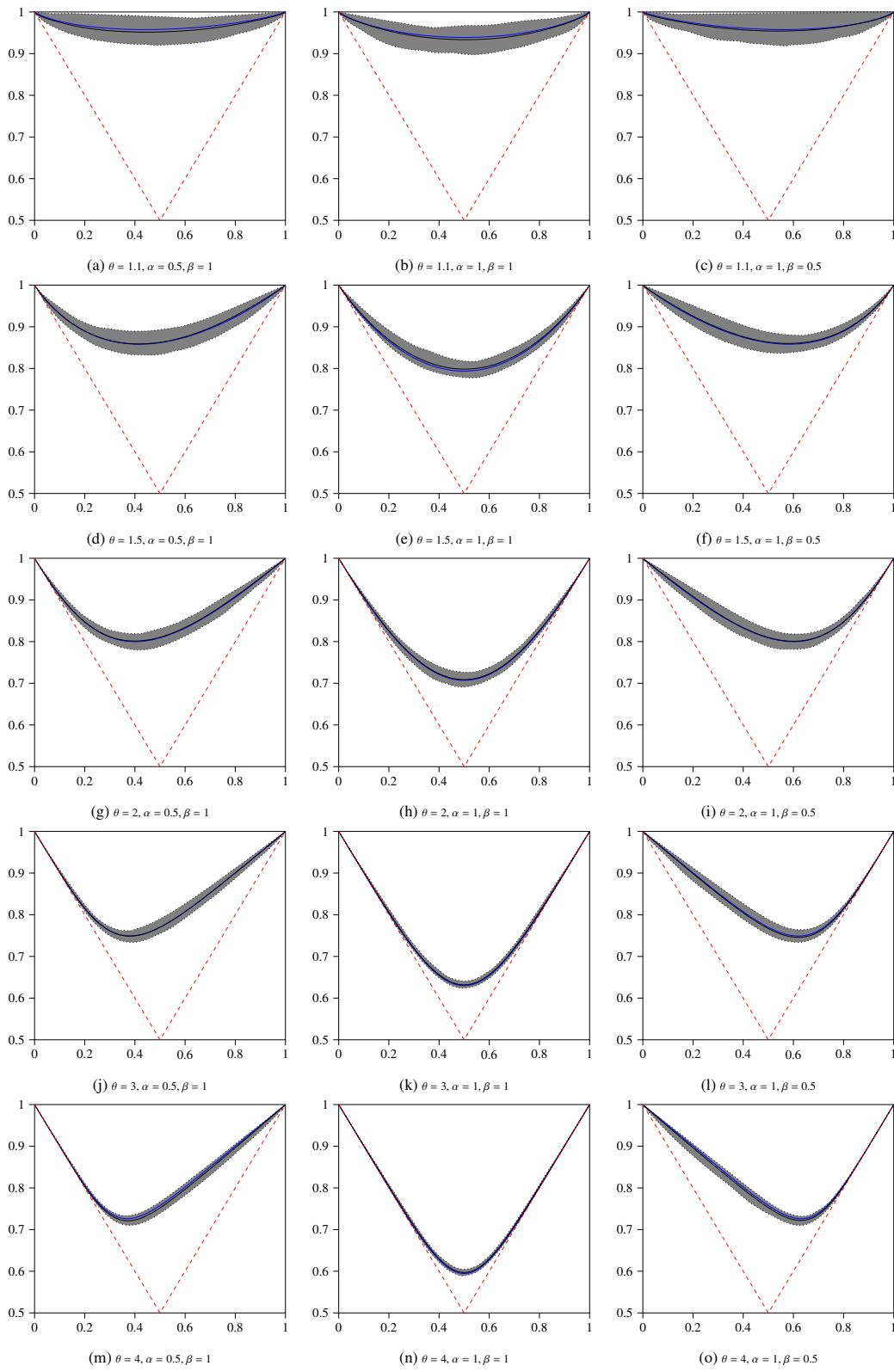


Figure 11: Simulation study for the Gumbel family. The blue line designates the ground-truth PF, whereas the black corresponds to the estimations' pointwise mean. The shaded areas represent 98% pointwise confidence intervals for the estimates.

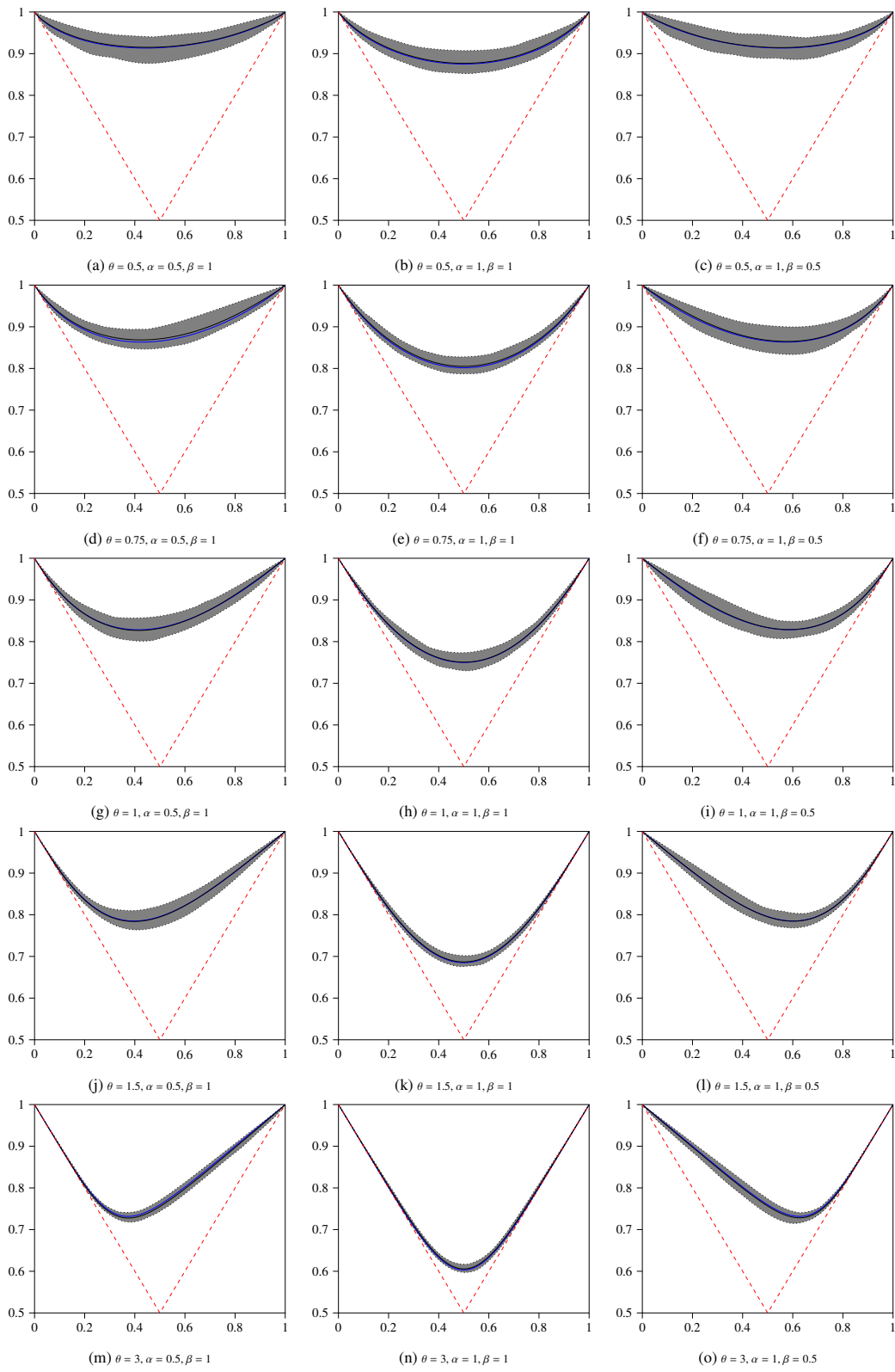


Figure 12: Simulation study for the Galambos family. The blue line designates the ground-truth PF, whereas the black corresponds to the estimations' pointwise mean. The shaded areas represent 98% pointwise confidence intervals for the estimates.



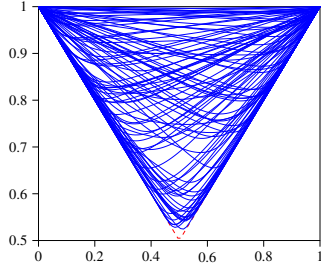


Figure 13: A subsample of size 100 from the whole population of random PFs used in the second part of the SS.

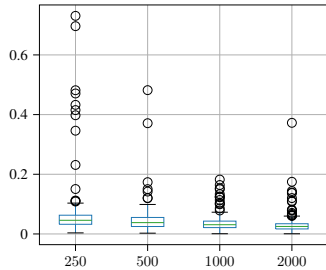


Figure 14: Box plots of the TVD distributions for each sample size.

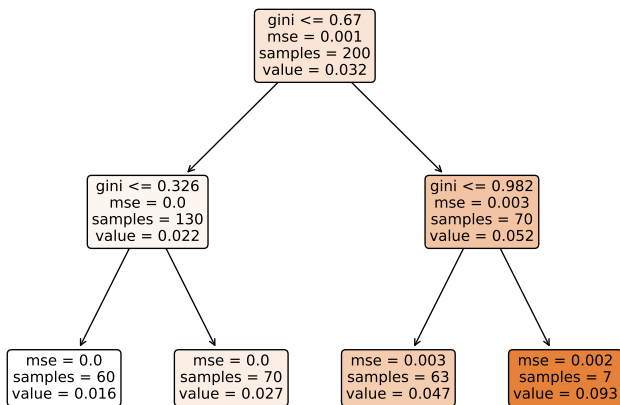


Figure 15: Regression tree (depth 2) of TVD on the GC for sample size 2,000. On average, our method performs well even on the seven instances with GC above 98%.

#### 4.3.1. Context

In the year 2015, the LIGO<sup>9</sup> Scientific Collaboration and the Virgo Collaboration announced the first direct detection of a gravitational wave (GW), produced by the merger of a binary black hole [49]. The existence of GWs, ripples in the fabric of space-time, was predicted by Einstein's theory of general relativity in 1916 [50] as a mathematical construct that many thought to have no physical meaning. It took nearly a century from its prediction and 60 years of search to experimentally ascertain the discovery, opening a new era for astronomy.

Only the most extreme events in the Universe, in terms of energy, can generate GWs strong enough to be detected by current experimental procedures, due to the small value of the gravitational constant [50], which expresses the rigidity of space-time. A significant amount of human and material resources is needed to detect GWs. Specifically, sufficiently sensitive interferometers need to have arms several kilometres long. Additionally, in order to discriminate between true detections and spurious local signals (like electromagnetic radiation or earthquakes), several detectors, far apart from each other, are needed.

LIGO, settled in the United States, with two laboratories, was the first detector of an advanced global network that aims to increase the accuracy and the exhaustiveness of discoveries [49], soon to be joined by others, most notably Virgo, in Italy. Despite LIGO and Virgo joining efforts, it was LIGO that reported the first detection since the Virgo facilities were not operating at that time for upgrading reasons. Since the first detection in 2015, the collaboration of LIGO and Virgo has confirmed 50 events. All of them correspond to massive body mergers, mainly black holes and neutron stars.

#### 4.3.2. Data

We have chosen the GW detection dataset gathered by the LIGO and Virgo collaborations during their first three observation runs to test the applicability of our method. It consists of 50 rows and two columns. Each row represents a merger event, while each column features one of the masses involved in the event, measured in solar mass units ( $M_{\odot}$ ). During the first and second observation runs, 11 events were detected, while the third run provided 39. The first event was GW150914, in September 2015, and the last one, GW190930\_133541, in September 2019. LIGO and Virgo report the larger of the two masses, the primary mass, as the first tuple component, followed by the secondary mass.

We believe that very few datasets better represent bivariate data, considering the very nature of binary mergers. Bivariate models are usually building blocks for higher-dimensional ones, but in this case, all the attention is focused on two mass values, of high scientific relevance. Another aspect that adds to this significance is the scarcity of data, for only 50 events have been recorded during five years. This scarcity contrasts with the increasingly large amounts of information coming from IoT, social networks, finance, among others, in the current era of Big Data.

<sup>9</sup>Laser Interferometer Gravitational-Wave Observatory.

### 4.3.3. Disclaimer

The purpose of this section is to test our method on real-world data. We have not counted on any physics expert to assess the relevance of our results. On the contrary, we have preferred to see data from an amateur perspective, as one of the goals of our method is exploratory data analysis. To gain a deeper understanding of the physical phenomena, professional researchers use parametric models grounded on a solid theoretical base [51]. The physics research community should take our results with caution in this respect.

### 4.3.4. Model

As mentioned above, the dataset consists of 50 bivariate observations  $\mathcal{D} = \{(M_1^{(i)}, M_2^{(i)})\}_{i=1}^{50}$ , where  $M_1^{(i)} \geq M_2^{(i)}$ . The last censoring constraint makes the dataset not directly tractable by our method, best suited for copulas supported on the whole  $[0, 1]^2$ , unless conveniently preprocessed.

LIGO and Virgo perform a statistical analysis of the joint mass distribution in [51]. To do so, they consider two separate univariate models. The first one, models the primary mass  $M_1$  unchanged, whereas the second one models the *mass ratio*  $Q = M_2/M_1$  conditioning on  $M_1$ . Since  $M_1 \geq M_2$ , by definition, the resulting model captures by construction the censoring constraint. The final joint model is formed by the vector  $(M_1, QM_1)$ .

Instead of considering a ratio variable to be later multiplied by the primary mass to calculate the secondary mass, we will directly tackle the modelling of a bivariate mass vector. To apply our method, we turned the censoring problem into an exchangeable one, where both masses played the same role. Of course, the original dataset  $\mathcal{D}$  does not allow such a treatment, so we had to hypothesize a new sample space where primary masses are detected with 50% probability at the first vector component and 50% at the second one. Such a scenario would occur if detections of an event reported masses indistinctly of their relative order.

Regardless of its physical significance, considering both masses indistinctly would allow us to fit a single univariate model shared by both masses, which, in turn, would help to focus on the main purpose of our experiment, the bivariate dependency, reducing the overall model complexity. Later on, we would find out that a bivariate mass model was indeed a much more interesting and tractable problem with the tools of EVCs at our hands.

To perform such an analysis, we built a new sample  $\tilde{\mathcal{D}} = \{(\tilde{M}_1^{(i)}, \tilde{M}_2^{(i)})\}_{i=1}^{100}$ , where, for  $j = 1, 2$ ,  $\tilde{M}_j^{(i)} = M_j^{(i)}$ , if  $i \leq 50$ , and  $\tilde{M}_j^{(i)} = M_{1+j \bmod 2}^{(i-50)}$ , if  $i > 50$ . Using the previous up-sampled and symmetrical dataset, we fitted (i) a single univariate mass model  $f$  for both margins and (ii) a copula model  $C$  of the dependency between mass ranks. Note that the number of observations available for model fitting doubled with the transformed sample, which could help overcome data scarcity.

With these tools, we targeted a random vector  $(\tilde{M}_1, \tilde{M}_2)$ . In order to retrieve the original primary-secondary mass model, we just had to take  $M_1 = \max\{\tilde{M}_1, \tilde{M}_2\}$  and  $M_2 = \min\{\tilde{M}_1, \tilde{M}_2\}$ .

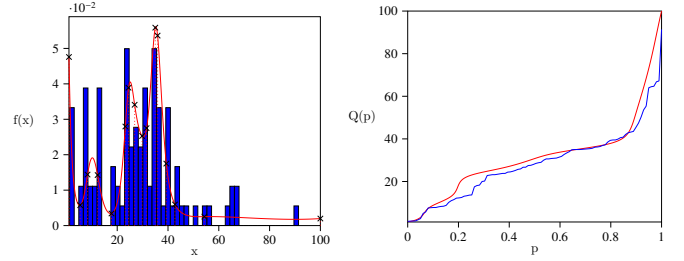


Figure 16: Univariate margin mass model. The pdf is displayed on the left, whereas the quantile function is on the right. In both cases, the fitted model shows in red and the empirical estimate is in blue. The vertical cuts on the left correspond to the underlying spline knots.

*Univariate margin model.* We decided to employ a semiparametric model for the univariate margin mass model to make up for our lack of expertise concerning stellar masses. We first considered using Kernel Density Estimation but eventually discarded it because the mass variables were bounded. Then, we successfully tried the same technique we used for modelling the density  $f$  in (17): Bayes space pdfs built from ZBSs.

The result of our experiment is shown in Figure 16. We selected 17 parameters, with knots distributed according to the original sample between  $1 M_\odot$  and  $100 M_\odot$ , and a curvature penalty factor of 10. The first mode, near  $1 M_\odot$ , mostly corresponds to neutron stars; black hole masses typically range beyond  $5 M_\odot$ .

*Bivariate copula model.* Letting  $\hat{F}$  be the empirical CDF of the univariate sample  $\{\tilde{M}_1^{(i)}\}_{i=1}^{100}$  (equivalently, from  $\{\tilde{M}_2^{(i)}\}_{i=1}^{100}$ ), we decided to fit a copula pseudo-sample  $\tilde{\mathcal{D}}_{\text{cop}} = \{(\tilde{U}_1^{(i)}, \tilde{U}_2^{(i)})\}_{i=1}^{100} = \{(\hat{F}(\tilde{M}_1^{(i)}), \hat{F}(\tilde{M}_2^{(i)}))\}_{i=1}^{100}$  independent of the fitted margin model from the previous section.

The applicability of EVCs was readily made clear after inspecting  $\tilde{\mathcal{D}}_{\text{cop}}$ , where the mirrored data points resembled some characteristic patterns we saw during a random EVC generation phase. Namely, they outlined two curved paths that met at both the lower and upper tail corners. The correlation was also relatively high, which, according to [8], would narrow down the range of admissible PFs, reducing variance.

However, data inspection also revealed the absence of upper tail dependence, while lower tail dependence was present. This behaviour did not match the features of EVCs: in practice, they never have lower tail dependence, but they do exhibit dependence in the upper tail. Interestingly, we can resort to *survival copulas* whenever a switch between lower and upper tails is needed, as recommended in [7]. If a random vector with uniform margins  $(U, V)$  is distributed according to a copula  $C$ , then  $(1 - U, 1 - V)$  follows the survival copula [2, 52]  $\check{C}(u, v) = u + v - 1 + C(1 - u, 1 - v)$ . The bivariate copula sample  $\tilde{\mathcal{D}}_{\text{cop}}$  was accordingly transformed into  $\tilde{\mathcal{D}}_{\text{surv}} = \{(1 - \tilde{U}_1^{(i)}, 1 - \tilde{U}_2^{(i)})\}_{i=1}^{100}$ . Of course, once  $\check{C}$  fits  $\tilde{\mathcal{D}}_{\text{surv}}$ , the original copula can be retrieved by taking  $C$  equal to the survival copula of  $\check{C}$ .

An extreme-value dependence test [53], implemented in the function `evTestK` of the R package `copula` [54, 55, 56, 57], confirmed our intuition about the applicability of EVCs, yielding a p-value higher than 0.35.

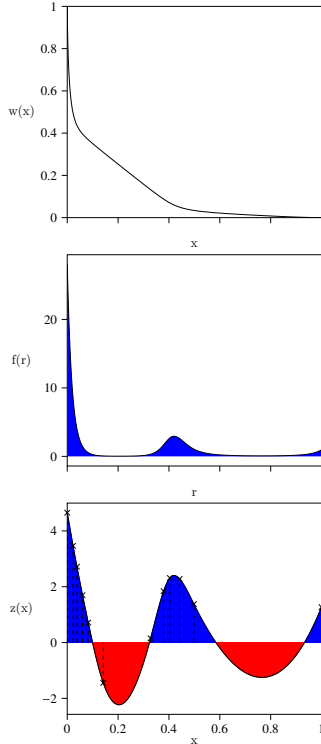


Figure 17: Internal function constructs  $z$  (zero-integral spline),  $f$  (Bayes density) and  $W$  (WT). The plot displays the underlying spline knots of  $z$ .

The copula model builds upon a cubic (orthonormal) ZBS basis with 13 elements, a curvature penalty factor of  $10^{-5}$  and interpolation grid sizes of  $k+2 = 80$ , in Algorithm 3, and  $n+2 = 200$ , in Algorithm 2. The value of the latter setting is lower than the one employed in the SS based on the reduced sample size.

Figure 17 shows the final state of the internal functions defined in the WT domain. As we can see, the resulting Bayes density is bimodal, yielding a WT with an almost linear region. On the other hand, Figure 18 shows the estimated PF and its correspondent  $h$  density (30). Despite the sample  $\tilde{\mathcal{D}}_{\text{surv}}$  being exchangeable, the  $h$  estimate fails to be perfectly symmetrical, with the left peak a bit higher than the one on the right. This behaviour was not wholly unexpected, given that our method does not address symmetry specifically. Taking that into account, Figure 18 shows that symmetry is reasonably well captured. Notwithstanding, before reversing the survival model, we decided to apply a symmetrization procedure on the resulting PF  $A$ , considering  $\tilde{A}(t) = [A(t) + A(1-t)]/2$ .

Figure 19 shows the result of the Bayesian posterior distribution of PFs, using the previous *maximum a posteriori* estimate as an initial guess for the MCMC sampling. We drew a million random observations from the posterior distribution. The job was divided into 100 *Spark* tasks corresponding to MCMC runs with 100 independent walkers [28], each one generating 200 observations, with a *burn-in* period of 100. The confidence interval turned out to be wider than expected but preserving the overall shape.

Finally, Figure 20 shows a sample-density plot of the final copula after symmetrization and reversal of the survival trans-

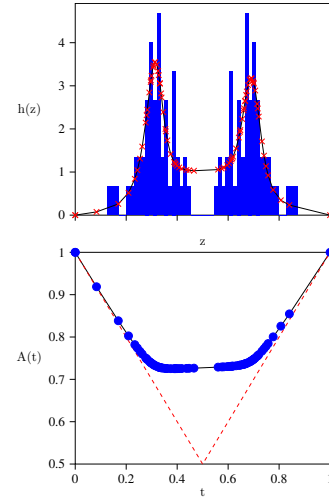


Figure 18: PF  $A$  and target density  $h$ . The knots represent the function values at the  $t_i$ 's grid defined in Algorithm 3.

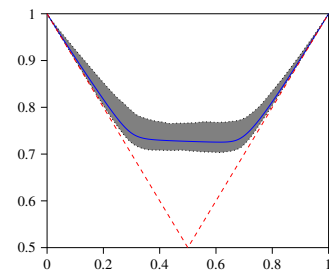


Figure 19: Pointwise confidence interval (98%) and mean of the posterior PFs sample from the MCMC simulation.

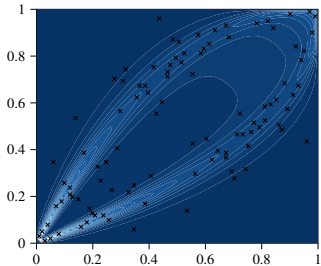


Figure 20: Final copula pdf after symmetrization and reversal of the survival transformation. The data points shown belong to the  $\tilde{\mathcal{D}}_{\text{cop}}$  dataset.

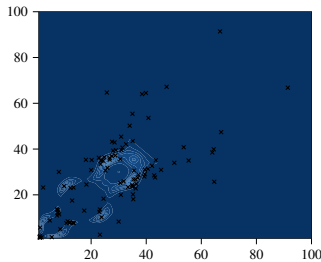


Figure 21: Joint pdf for the final model. The data points shown belong to the  $\tilde{\mathcal{D}}$  dataset.

formation. The pdf captures the presence of lower tail dependence and the absence of upper tail dependence. Also, there exists a remarkable density gap in the region surrounding the diagonal  $\{u = v\}$ , which means that BMs involving similar masses are rare.

*Joint model.* Once fitted both the univariate margin mass model (ZBSs) and the copula model (survival symmetrical EVC), the final joint model immediately followed. Figure 21 shows the joint density of the final model. On the other hand, Figure 22 plots the original LIGO-Virgo dataset against a random sample generated from the previous model, where the first and second components are the maximum and the minimum, respectively, to match the original dataset criterion, as mentioned earlier. There are ten times more random samples than original data points, for a total of 500. Our model captures three main clusters, concentrated in the regions  $[0, 20]^2$ ,  $[20, 40] \times [0, 20]$  and  $[20, 40]^2$ . It is also worth mentioning that there seems to be a barrier at  $\{M_2 = 40\}$ . Overall, the latter is probably the most unexpected prediction of our model, in contrast to the reported models in [51], and a clear sign of *overfitting*: 30 parameters (17 univariate + 13 copula) for only 50 observations (100 after up-sampling).

## 5. Discussion

In section 3, we introduced a new semiparametric method for EVC estimation, along with some theoretical and practical results. Namely, EVCs built using our method have interesting convergence and dependence properties that relate to an inner pdf that is at the core of the construction.

In section 4.2, we presented the results of a thorough SS consisting of two independent parts. In the first one, we repeat-

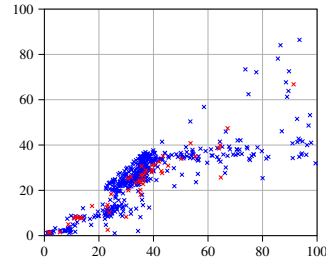


Figure 22: Original masses (red) against random samples from our model (blue).

edly performed estimations on random samples from 30 different EVCs, with varying degrees of concordance and asymmetry, concluding that our method is effective from a bias-variance tradeoff perspective. If any, slight biases appeared on low concordance and asymmetrical samples, which could be expected from theoretical results [8]. On the other hand, the second part of the simulation stressed our method, as it was applied on 200 random EVCs and evaluated according to a conservative metric like TVD. Our method generally performed very well, producing small TVD values with respect to ground truth over the whole GC range, including highly correlated samples. Additionally, performance improved as sample sizes increased. The only issue encountered relates to numerical instabilities that might hinder the estimation process on rare occasions due to the numerous approximations, especially for extremely high correlations.

In section 4.3, we tested our method on actual data from an exceptional origin: the LIGO and Virgo BM detections. The underlying dependence structure was consistent with the extreme-value hypothesis, according to a statistical test. After fitting a flexible univariate model for both margins, we fitted an EVC for the survival version of the data points. Our method proved to be flexible enough to capture a peculiar bimodal shape. Overall, the fitted model produced a very convincing synthetic dataset for BMs.

The main contribution of our work is the proposal of a new semiparametric estimator that allows fitting parameters of an EVC in a fully unconstrained manner. Our construction allows generating random EVCs at will, with all the theoretical constraints automatically ensured.<sup>10</sup> To do so, we rely on fundamental but powerful transformations that eliminate all the stringent constraints imposed by the PF. Thanks to this flexible and straightforward procedure, EVCs could be studied, for instance, in the context of information geometry as finite-dimensional objects. Finally, we demonstrated the feasibility of our approach, showing that, despite all the operations involved, likelihood-based optimization can be successfully and efficiently performed with the available software tools and algorithms.

Our method opens up exciting possibilities for data analysis. Being semiparametric, it provides a convenient balance between bias and variance. As we have demonstrated, our esti-

<sup>10</sup>As demonstrated in the second part of the SS.

mator subsumes two well-known parametric EVC families, as well as many other randomly generated instances. Compared to parametric models, our approach has a niche as a *silver bullet*. On the other hand, it provides a sure path to complying with PF constraints, even for small samples like LIGO and Virgo's. Nonparametric models will generally struggle in such settings. Nevertheless, they will have an edge for asymptotically large samples.

## 6. Future work

Research could continue in several varied ways. A straight research line could demonstrate the applicability of the combination of ZBSs and WTs in the context of semiparametric models for bivariate ACs [3], as an alternative to [19] or other Laplace transform-based methods. Precisely, McNeil and Nešlehová introduced Williamson's transform to characterize multivariate ACs and an extension of these: Liouville copulas [22]. Also related to ACs, the very same form introduced in this paper would fit the specific case of Lorenz copulas [23].

Also, our method could be conveniently modified to incorporate deep learning approaches. Instead of ZBSs, an over-parameterized multilayer perceptron could be employed, at the risk of losing identifiability and incurring in overfitting. Alternatively, we could follow a similar approach to [58], where a deep neural network architecture mimics the Laplace transform structure of an AC, in the context of EVCs and over Williamson's transform, instead.

A third research line could combine the developed semiparametric and deep learning techniques for EVCs and ACs in an attempt to model the more expressive Archimax [5] family, which is a superset of both.

Without going any further, there are some aspects of our method that would benefit from more profound research. In particular, the fixed slope values of the resulting PF become a barrier that prevents from achieving a fully flexible semiparametric model. Although we proposed a solution based on Khoudraji's device, there remain questions on its applicability in practice. Namely, a review of gradient-free optimization methods and their suitability for such a task would be mandatory. Additionally, on the implementation side, developing a reliable and accurate initial guess mechanism would also help to improve execution times even more, especially for highly correlated samples.

Last but not least, it would be interesting to see how our method compares to other approaches in a thorough review like [12].

## Acronyms

**AC** Archimedean copula. 3, 5, 22

**BM** binary merger. 18, 20, 21

**CDF** cumulative distribution function. 1, 2, 6, 10, 11, 19

**CLR** centred log-ratio. 7, 10

**EVC** extreme-value copula. 1–3, 5, 6, 8–10, 13–15, 18–22

**GC** Gini coefficient. 10, 15, 18, 21

**GW** gravitational wave. 18

**iff** if and only if. 1, 2, 5, 6, 10

**pdf** probability density function. 6–10, 12, 14, 15, 19–21

**PF** Pickands function. 1–5, 7–22

**rv** random variable. 5–7, 10

**SS** simulation study. 2, 13–15, 18, 20, 21

**TVD** total variation distance. 8, 9, 14, 15, 18, 21

**WT** Williamson transform. 5–11, 13, 20, 22

**ZBS** zero-integral B-spline. 7–11, 14, 19, 20, 22

## References

- [1] Roger B. Nelsen. *An Introduction to Copulas*. Springer New York, Nov. 19, 2010. 288 pp. ISBN: 1441921095. URL: [https://www.ebook.de/de/product/13633887/roger\\_b\\_nelsen\\_an\\_introduction\\_to\\_copulas.html](https://www.ebook.de/de/product/13633887/roger_b_nelsen_an_introduction_to_copulas.html).
- [2] Eric Bouyé et al. "Copulas for Finance - A Reading Guide and Some Applications". In: *SSRN Electronic Journal* (2000). DOI: 10.2139/ssrn.1032533.
- [3] Alexander J. McNeil and Johanna Nešlehová. "Multivariate Archimedean copulas, d-monotone functions and  $\ell_1$ -norm symmetric distributions". In: *The Annals of Statistics* 37.5B (Oct. 2009), pp. 3059–3097. DOI: 10.1214/07-aos556.
- [4] Gordon Gudendorf and Johan Segers. "Extreme-Value Copulas". In: *Copula Theory and Its Applications*. Springer Berlin Heidelberg, 2010, pp. 127–145. DOI: 10.1007/978-3-642-12465-5\_6.
- [5] A. Charpentier et al. "Multivariate Archimax copulas". In: *Journal of Multivariate Analysis* 126 (Apr. 2014), pp. 118–136. DOI: 10.1016/j.jmva.2013.12.013.
- [6] Simon Guillotte and François Perron. "Polynomial Pickands functions". In: *Bernoulli* 22.1 (Feb. 2016), pp. 213–241. DOI: 10.3150/14-bej656.
- [7] Patrick Eschenburg. "Properties of extreme-value copulas". MA thesis. 2013.
- [8] N. Kamnitsui et al. "On the size of the class of bivariate extreme-value copulas with a fixed value of Spearman's rho or Kendall's tau". In: *Journal of Mathematical Analysis and Applications* 472.1 (Apr. 2019), pp. 920–936. DOI: 10.1016/j.jmaa.2018.11.057. URL: <https://www.sciencedirect.com/science/article/pii/S0022247X18310035?via=ihub>.

- [9] Friedrich Schmid and Rafael Schmidt. “Nonparametric inference on multivariate versions of Blomqvist’s beta and related measures of tail dependence”. In: *Metrika* 66.3 (Dec. 2006), pp. 323–354. doi: 10.1007/s00184-006-0114-3.
- [10] A. Khoudraji. “Contributions à l’étude des copules et à la modélisation des valeurs extrêmes bivariées”. PhD thesis. Université Laval, Québec, Canada, 1995.
- [11] Jean-François Quessy and Othmane Kortbi. “Minimum-distance statistics for the selection of an asymmetric copula in Khoudraji’s class of models”. In: *Statistica Sinica* (2016). doi: 10.5705/ss.202014.0082.
- [12] Sabrina Vettori, Raphaël Huser, and Marc G. Genton. “A comparison of dependence function estimators in multivariate extremes”. In: *Statistics and Computing* 28.3 (May 2017), pp. 525–538. doi: 10.1007/s11222-017-9745-7.
- [13] James Pickands. “Multivariate extreme value distribution”. In: *Proceedings 43th, Session of International Statistical Institution, 1981* (1981).
- [14] Javier Rojo Jiménez, Enrique Villa-Diharce, and Miguel Flores. “Nonparametric Estimation of the Dependence Function in Bivariate Extreme Value Distributions”. In: *Journal of Multivariate Analysis* 76.2 (Feb. 2001), pp. 159–191. doi: 10.1006/jmva.2000.1931.
- [15] P. Capéraà, A. L. Fougères, and C. Genest. “A nonparametric estimation procedure for bivariate extreme value copulas”. In: *Biometrika* 84.3 (Sept. 1997), pp. 567–577. doi: 10.1093/biomet/84.3.567.
- [16] G. Marcon et al. “Multivariate nonparametric estimation of the Pickands dependence function using Bernstein polynomials”. In: *Journal of Statistical Planning and Inference* 183 (Apr. 2017), pp. 1–17. doi: 10.1016/j.jspi.2016.10.004.
- [17] Eric Cormier, Christian Genest, and Johanna Nešlehová. “Using B-splines for nonparametric inference on bivariate extreme-value copulas”. In: *Extremes* 17.4 (Aug. 2014), pp. 633–659. doi: 10.1007/s10687-014-0199-4.
- [18] John H. J. Einmahl and Johan Segers. “Maximum empirical likelihood estimation of the spectral measure of an extreme-value distribution”. In: *The Annals of Statistics* 37.5B (Oct. 2009). doi: 10.1214/08-aos677.
- [19] José Miguel Hernández-Lobato and Alberto Suárez. “Semiparametric bivariate Archimedean copulas”. In: *Computational Statistics & Data Analysis* 55.6 (June 2011), pp. 2038–2058. doi: 10.1016/j.csda.2011.01.018.
- [20] Gordon Gudendorf and Johan Segers. “Nonparametric estimation of multivariate extreme-value copulas”. In: *Journal of Statistical Planning and Inference* 142.12 (Dec. 2012), pp. 3073–3085. doi: 10.1016/j.jspi.2012.05.007.
- [21] Tomáš Bacigál. “On Some Applications of Williamson’s Transform in Copula Theory”. In: *Advances in Intelligent Systems and Computing*. Springer International Publishing, May 2017, pp. 21–30. doi: 10.1007/978-3-319-59306-7\_3.
- [22] Alexander J. McNeil and Johanna Nešlehová. “From Archimedean to Liouville copulas”. In: *Journal of Multivariate Analysis* 101.8 (Sept. 2010), pp. 1772–1790. doi: 10.1016/j.jmva.2010.03.015.
- [23] Andrea Fontanari, Pasquale Cirillo, and Cornelis W. Oosterlee. “Lorenz-generated bivariate Archimedean copulas”. In: *Dependence Modeling* 8.1 (Jan. 2020), pp. 186–209. doi: 10.1515/demo-2020-0011. URL: <https://www.degruyter.com/document/doi/10.1515/demo-2020-0011/html>.
- [24] J. J. Egozcue, J. L. Díaz-Barrero, and V. Pawłowsky-Glahn. “Hilbert Space of Probability Density Functions Based on Aitchison Geometry”. In: *Acta Mathematica Sinica, English Series* 22.4 (Jan. 2006), pp. 1175–1182. doi: 10.1007/s10114-005-0678-2.
- [25] Jitka Machalová et al. “Compositional splines for representation of density functions”. In: *Computational Statistics* (Oct. 2020). doi: 10.1007/s00180-020-01042-7.
- [26] R. M. Corless et al. “On the LambertW function”. In: *Advances in Computational Mathematics* 5.1 (Dec. 1996), pp. 329–359. doi: 10.1007/bf02124750.
- [27] Carl de Boor. “Spline Basics”. In: *Handbook of Computer Aided Geometric Design*. Elsevier, 2002, pp. 141–163. doi: 10.1016/b978-044451104-1/50007-1.
- [28] Daniel Foreman-Mackey et al. “emcee: The MCMC Hammer”. In: *Publications of the Astronomical Society of the Pacific* 125.925 (Mar. 2013), pp. 306–312. doi: 10.1086/670067.
- [29] Alexandre B. Tsybakov. *Introduction to Nonparametric Estimation*. Springer New York, 2009. doi: 10.1007/b13794.
- [30] Amélie Fils-Villetard, Armelle Guillou, and Johan Segers. “Projection estimators of Pickands dependence functions”. In: *Canadian Journal of Statistics* 36.3 (Sept. 2008), pp. 369–382. doi: 10.1002/cjs.5550360303.
- [31] William C. Waterhouse. “Uniform Convergence and Graph Convergence”. In: *The American Mathematical Monthly* 83.8 (Oct. 1976), p. 641. doi: 10.2307/2319894.
- [32] Volker Schmitz. “Copulas and Stochastic Processes”. PhD thesis. Aachen: Rheinisch-Westfälischen Technischen Hochschule Aachen, Jan. 21, 2003. ISBN: 3-8322-1278-7. URL: <https://d-nb.info/972691669/34>.
- [33] Gabriel Doyon. “On Densities of Extreme Value Copulas”. MA thesis. Universität Zürich, 2013.

- [34] Sándor Guzmics and Georg Ch. Pflug. “A new extreme value copula and new families of univariate distributions based on Freund’s exponential model”. In: *Dependence Modeling* 8.1 (Jan. 2020), pp. 330–360. doi: 10.1515/demo-2020-0018.
- [35] Dougal Maclaurin, David Duvenaud, and Ryan P. Adams. “Autograd: Effortless gradients in numpy”. In: *ICML 2015 AutoML Workshop*. Vol. 238. 2015, p. 5.
- [36] Larry I. Schumaker. “On Shape Preserving Quadratic Spline Interpolation”. In: *SIAM Journal on Numerical Analysis* 20.4 (Aug. 1983), pp. 854–864. doi: 10.1137/0720057.
- [37] G. E. Alefeld, F. A. Potra, and Yixun Shi. “Algorithm 748: enclosing zeros of continuous functions”. In: *ACM Transactions on Mathematical Software* 21.3 (Sept. 1995), pp. 327–344. doi: 10.1145/210089.210111.
- [38] Richard H. Byrd et al. “A Limited Memory Algorithm for Bound Constrained Optimization”. In: *SIAM Journal on Scientific Computing* 16.5 (Sept. 1995), pp. 1190–1208. doi: 10.1137/0916069.
- [39] Javier Fernández Serrano. “Modelling Multivariate Dependencies with Semiparametric Archimedean Copulas”. MA thesis. Madrid: Universidad Autónoma de Madrid, July 8, 2016, p. 172. URL: <http://hdl.handle.net/10486/676101>.
- [47] Christian Genest and Johanna Nešlehová. “When Gumbel met Galambos”. In: *Copulas and Dependence Models with Applications*. Springer International Publishing, 2017, pp. 83–93. doi: 10.1007/978-3-319-64221-5\_6.
- [48] Christian Genest, Johanna Nešlehová, and Jean-François Quessy. “Tests of symmetry for bivariate copulas”. In: *Annals of the Institute of Statistical Mathematics* 64.4 (Sept. 2011), pp. 811–834. doi: 10.1007/s10463-011-0337-6.
- [49] B. P. Abbott et al. “Observation of Gravitational Waves from a Binary Black Hole Merger”. In: *Physical Review Letters* 116.6 (2016). doi: 10.1103/physrevlett.116.061102.
- [50] Jorge Cervantes-Cota, Salvador Galindo-Uribarri, and George Smoot. “A Brief History of Gravitational Waves”. In: *Universe* 2.3 (Sept. 2016), p. 22. doi: 10.3390/universe2030022.
- [51] R. Abbott et al. “Population Properties of Compact Objects from the Second LIGO–Virgo Gravitational-Wave Transient Catalog”. In: *The Astrophysical Journal Letters* 913.1 (May 2021), p. L7. doi: 10.3847/2041-8213/abe949.
- [52] Pierre Georges et al. “Multivariate Survival Modelling: A Unified Approach with Copulas”. In: *SSRN Electronic Journal* (2001). doi: 10.2139/ssrn.1032559.
- [53] Noomen Ben Ghorbal, Christian Genest, and Johanna Nešlehová. “On the Ghoudi, Khoudraji, and Rivest test for extreme-value dependence”. In: *Canadian Journal of Statistics* 37.4 (Dec. 2009), pp. 534–552. doi: 10.1002/cjs.10034.
- [54] Marius Hofert et al. *copula: Multivariate Dependence with Copulas*. R package version 1.0-1. 2020. URL: <https://CRAN.R-project.org/package=copula>.
- [55] Ivan Kojadinovic and Jun Yan. “Modeling Multivariate Distributions with Continuous Margins Using the copula R Package”. In: *Journal of Statistical Software* 34.9 (2010), pp. 1–20. URL: <https://www.jstatsoft.org/v34/i09/>.
- [56] Jun Yan. “Enjoy the Joy of Copulas: With a Package copula”. In: *Journal of Statistical Software* 21.4 (2007), pp. 1–21. URL: <https://www.jstatsoft.org/v21/i04/>.
- [57] Marius Hofert and Martin Mächler. “Nested Archimedean Copulas Meet R: The nacopula Package”. In: *Journal of Statistical Software* 39.9 (2011), pp. 1–20. URL: <https://www.jstatsoft.org/v39/i09/>.
- [58] Chun Kai Ling, Fei Fang, and J. Zico Kolter. “Deep Archimedean Copulas”. In: *34th Conference on Neural Information Processing Systems (NeurIPS 2020)*. Vancouver, Canada, Dec. 5, 2020. arXiv: 2012.03137 [cs.LG].

## Resources

- [40] Docker, Inc. *Docker. Container technology*. URL: <https://www.docker.com/> (visited on 09/11/2021).
- [41] The Cloud Native Computing Foundation. *Kubernetes. Production-Grade Container Scheduling and Management*. URL: <https://kubernetes.io/> (visited on 09/11/2021).
- [42] The minikube community. *minikube. Run Kubernetes locally*. URL: <https://minikube.sigs.k8s.io/> (visited on 10/04/2021).
- [43] The Apache Software Foundation. *Spark. A unified analytics engine for large-scale data processing*. Version 3.1.1. Mar. 2, 2021. URL: <https://spark.apache.org/> (visited on 09/11/2021).
- [44] Data Mechanics. *Docker image for Apache Spark*. URL: <https://hub.docker.com/r/datamechanics/spark> (visited on 09/11/2021).
- [45] Google Cloud Platform. *Spark Operator. Kubernetes operator for managing the lifecycle of Apache Spark applications on Kubernetes*. URL: <https://operatorhub.io/operator/spark-gcp> (visited on 09/11/2021).
- [46] Argo Project. *Argo CD. Declarative continuous deployment for Kubernetes*. URL: <https://argoproj.github.io/argo-cd/> (visited on 09/11/2021).